

Annual Review of Nuclear and Particle Science The Search for Electroweakinos

Anadi Canepa,¹ Tao Han,² and Xing Wang³

¹Fermi National Accelerator Laboratory, Batavia, Illinois 60510, USA; email: acanepa@fnal.gov

Annu. Rev. Nucl. Part. Sci. 2020. 70:425-54

The Annual Review of Nuclear and Particle Science is online at nucl.annualreviews.org

https://doi.org/10.1146/annurev-nucl-031020-121031

Copyright © 2020 by Annual Reviews. This work is licensed under a Creative Commons Attribution 4.0 International License, which permits unrestricted use, distribution, and reproduction in any medium, provided the original author and source are credited. See credit lines of images or other third party material in this article for license information

ANNUAL CONNECT

www.annualreviews.org

- · Download figures
- · Navigate cited references
- Keyword search
- Explore related articles
- · Share via email or social media

Keywords

SUSY, electroweakinos, WIMP dark matter, LHC

Abstract

In this review, we consider a general theoretical framework for fermionic color-singlet states—including a singlet, a doublet, and a triplet under the Standard Model SU(2)_L gauge symmetry, corresponding to the bino, higgsino, and wino in supersymmetric theories—generically dubbed electroweakinos for their mass eigenstates. Depending on the relations among these states' three mass parameters and their mixing after the electroweak symmetry breaking, this sector leads to a rich phenomenology that may be accessible in current and near-future experiments. We discuss the decay patterns of electroweakinos and their observable signatures at colliders, review the existing bounds on the model parameters, and summarize the current statuses of the comprehensive searches by the ATLAS and CMS Collaborations at the Large Hadron Collider. We also comment on the prospects for future colliders. An important feature of the theory is that the lightest neutral electroweakino can be identified as a weakly interacting massive particle cold dark matter candidate. We take into account the existing bounds on the parameters from the dark matter direct detection experiments and discuss the complementarity of the electroweakino searches at colliders.



² Department of Physics and Astronomy, University of Pittsburgh, Pittsburgh, Pennsylvania 15260, USA; email: than@pitt.edu

³ Department of Physics, University of California, San Diego, La Jolla, California 92093, USA; email: xiw006@physics.ucsd.edu

Contents 1. INTRODUCTION 2.4. Simplified Model and Phenomenological Minimal Supersymmetric 3. DARK MATTER RELIC DENSITY AND DIRECT 4.2. Production at Hadron Colliders and Next Lightest Supersymmetric

1. INTRODUCTION

The Higgs boson (*H*) discovered at the CERN Large Hadron Collider (LHC) by the ATLAS (1) and CMS (2) Collaborations completes the particle spectrum of the Standard Model (SM)—a self-consistent effective field theory that is valid up to an exponentially high scale. Yet, from the observational point of view, the SM is incomplete. The unexplained dark matter (DM), the lack of ingredients for generating the baryon–antibaryon asymmetry, and the inability to account for neutrino masses all imply the existence of physics beyond the Standard Model (BSM). Nevertheless, theoretical considerations—such as the hierarchy puzzle between the electroweak scale and the Planck scale (3–6), gauge coupling unification (7–10), new space-time symmetry (11–16), new strong dynamics (17–19), and warped extra dimensions (20, 21)—all indicate the need for New Physics at a scale not far from the electroweak scale (22–26). Therefore, the search for TeV-scale New Physics in experiments at the energy frontier continues to be a high priority for particle physics in the coming decades.

Current measurements of the Higgs boson properties at the LHC support the interpretation of it as an SM-like, weakly coupled elementary particle. In this regard, weak-scale supersymmetry (SUSY) may be the most compelling incarnation for New Physics at the next scale. The introduction of the new space-time symmetry requires the existence of SUSY partners of the SM particles with predictable couplings and will lead to profound theoretical and experimental implications. The pressing question concerns the unknown mechanism for SUSY breaking and the associated scale that determines the mass spectrum for the SUSY partners—preferably not much heavier than the electroweak scale. If the weak-scale SUSY is realized in nature, definitive confirmation will require discovery of the SUSY partners, such as the QCD colored states, including gluinos (\tilde{g}) and squarks (\tilde{q}) , and the electroweak partners, including the gauginos (\tilde{B}, \tilde{W}) and higgsinos

 (\tilde{H}) , or their mass eigenstates, the charginos $(\tilde{\chi}_i^\pm)$ and neutralinos $(\tilde{\chi}_j^0)$. Here and henceforth, we refer to these states generically as electroweakinos. If a discrete symmetry (called R parity) that classifies the SM particles (R even) and the SUSY partners (sparticles, R odd) is conserved, then the SUSY particles must be produced in pairs, and the lightest supersymmetric particle (LSP)—most commonly the lightest neutralino—will be practically stable. Such a stable neutral particle is weakly interacting and thus leads to a missing momentum signature in collider experiments. It is particularly interesting to note that such a weakly interacting massive particle (WIMP) will be a natural cold DM candidate (27). Thus, the search for SUSY at colliders is especially important because of the connection to DM detection.

Given an underlying theory of SUSY breaking and a mechanism for mediating the breaking effects to the SM sector, SUSY partner masses may be calculable in terms of the SUSY breaking scale. The null results from SUSY searches performed at the LHC to date,1 especially those in final states with substantial missing transverse momentum ($p_{\rm T}^{\rm miss}$) plus large hadronic activities, imply that the colored SUSY particles under QCD strong interaction may not have been copiously produced. With some simple assumptions, the interpretation of the current LHC data leads to the multi-TeV mass bound for the gluinos and light-generation squarks, making their direct discovery at the LHC increasingly difficult because of the kinematic limitation from the total collision energy at the LHC. However, it is quite conceivable that the charginos and neutralinos in the electroweak sector could be significantly lighter than the colored SUSY partners, as argued in the scenarios of so-called natural SUSY (32-35). The direct production of electroweak SUSY particles at the LHC occurs at a lower rate (36), and the current direct search bounds are thus rather weak (37). In addition, some DM considerations favor models with nearly degenerate electroweakinos (38), making their identification more challenging (39) given the lack of substantial $p_{\rm T}^{\rm mis}$. Thus, there is strong motivation to target electroweakinos in hopes of extending the SUSY search coverage. In this review, we focus on electroweakinos and decouple the SUSY color and scalar states. Although we work in a framework of the minimal supersymmetric Standard Model (MSSM) because of its clarity and predictability, our analyses and conclusions will be equally applicable to other color-singlet fermionic states (such as BSM heavy leptons) of SU(2)_L singlets, doublets, and triplets with a conserved global quantum number to ensure the existence of a stable light neutral particle as the WIMP DM candidate.

The rest of this review is organized as follows. We first present the model setup in Section 2 by specifying the electroweakino states and the model parameters of their masses and mixing. This background sets the tone for the parameter coverage in the searches. In Section 3, we consider the DM direct detection and present the current bounds on the model parameters that will serve as qualitative guidance and targets in future searches. The main body of this review is presented in Section 4, where we first show the predicted production cross sections for electroweakinos at hadron colliders and their decay modes in various theoretical scenarios, then summarize the current bounds from LEP and the LHC, and finally comment on expectations for future colliders. We summarize the review and discuss some future prospects in Section 5.

2. MODEL SETUP

We start with the general BSM formulation with the new fermionic states of the SU(2)_L multiplets: a singlet \tilde{B} (bino), a triplet \tilde{W} (wino), and two doublets \tilde{H}_d and \tilde{H}_u (higgsinos), as in the gaugino

¹For more information regarding these searches, we refer readers to the comprehensive programs for ATLAS (28) and CMS (29) (see also, e.g., 30, 31).

and higgsino sectors in the MSSM, with three mass parameters as²

$$M_1$$
, M_2 , and μ .

The mass matrix for the neutral components in the gauge eigenstate basis of $\psi^0 = (\tilde{B}, \tilde{W}^0, \tilde{H}_d^0, \tilde{H}_u^0)$ is

$$M_{\tilde{N}} = \begin{pmatrix} M_1 & 0 & -c_{\beta}s_W m_Z & s_{\beta}s_W m_Z \\ 0 & M_2 & c_{\beta}c_W m_Z & -s_{\beta}c_W m_Z \\ -c_{\beta}s_W m_Z & c_{\beta}c_W m_Z & 0 & -\mu \\ s_{\beta}s_W m_Z & -s_{\beta}c_W m_Z & -\mu & 0 \end{pmatrix}, \qquad 2.$$

where s_W and c_W indicate $\sin \theta_W$ and $\cos \theta_W$, respectively (with θ_W being the weak mixing angle), and s_β and c_β indicate $\sin \beta$ and $\cos \beta$, respectively (with $\tan \beta = \langle \tilde{H}_u^0 \rangle / \langle \tilde{H}_d^0 \rangle$). Similarly, the mass matrix of the charged components in the basis of $\psi^{\pm} = (\tilde{W}^+, \tilde{H}_u^+, \tilde{W}^-, \tilde{H}_d^-)$ is

$$M_{\tilde{C}} = \begin{pmatrix} 0_{2\times 2} & X_{2\times 2}^T \\ X_{2\times 2} & 0_{2\times 2} \end{pmatrix}, \quad \text{with} \quad X_{2\times 2} = \begin{pmatrix} M_2 & \sqrt{2}s_\beta m_W \\ \sqrt{2}c_\beta m_W & \mu \end{pmatrix}.$$
 3.

After the diagonalization, we arrive at the neutral and charged mass eigenstates: the neutralinos $\tilde{\chi}_{i}^{0}$ (i = 1, 2, 3, 4) and the charginos $\tilde{\chi}_{i}^{\pm}$ (i = 1, 2), respectively, with increasing mass for a higher label i. We refer to these states generically as electroweakinos.

As such, $\tilde{\chi}_1^0$ is the lightest electroweakino, and we refer to it as the LSP. If an electroweakino carries a dominant component of a gaugino or higgsino with an approximate mass as a function of M_1, M_2 , or μ , we call the state bino-like, wino-like, or higgsino-like, respectively. Furthermore, if one of the three mass scales is significantly lower than the other two, the LSP could be essentially a pure bino, a pure wino, or a pure higgsino. In such cases, it has become customary to liberally label the nearly degenerate multiplets as wino LSPs or higgsino LSPs. Obviously, the LSP $\tilde{\chi}_1^0$ is most characteristic because it can produce missing momentum in collider experiments if R parity is conserved, and it serves as the WIMP DM candidate. However, the next lightest supersymmetric particles (NLSPs) can also be of special importance because they may govern the collider signatures by the production and subsequent decays to the LSP. In the rest of this section, we categorize the parameter configurations into several characteristic cases according to the nature of the LSPs and NLSPs, and we discuss their mass spectra.

2.1. Scenario 1: Bino Lightest Supersymmetric Particle

First, we consider the scenario in which M_1 is lower than the other two parameters, M_2 and μ . This is a quite generic scenario; the most common example is the minimal supergravity model (mSUGRA) with universal gaugino masses (40–46). The bino LSP is a gauge singlet Majorana state whose annihilation in the early Universe occurred through squark and slepton exchange. In the scope of this review, we assume that the scalar sector is heavy and thus decoupled. Therefore, a pure bino as the DM would lead to an overclosure of the Universe, and we consider its mixing with the wino and higgsino for the following two cases:

Scenario 1a
$$M_1 < M_2 < \mu$$
: $\tilde{\chi}_1^0$ bino-like LSP; $\tilde{\chi}_1^{\pm}$, $\tilde{\chi}_2^0$ wino-like NLSPs 4. Scenario 1b $M_1 < \mu < M_2$: $\tilde{\chi}_1^0$ bino-like LSP; $\tilde{\chi}_1^{\pm}$, $\tilde{\chi}_{2,3}^0$ higgsino-like NLSPs 5.

²Unless otherwise specified, M_1 , M_2 , and μ refer to their absolute values.

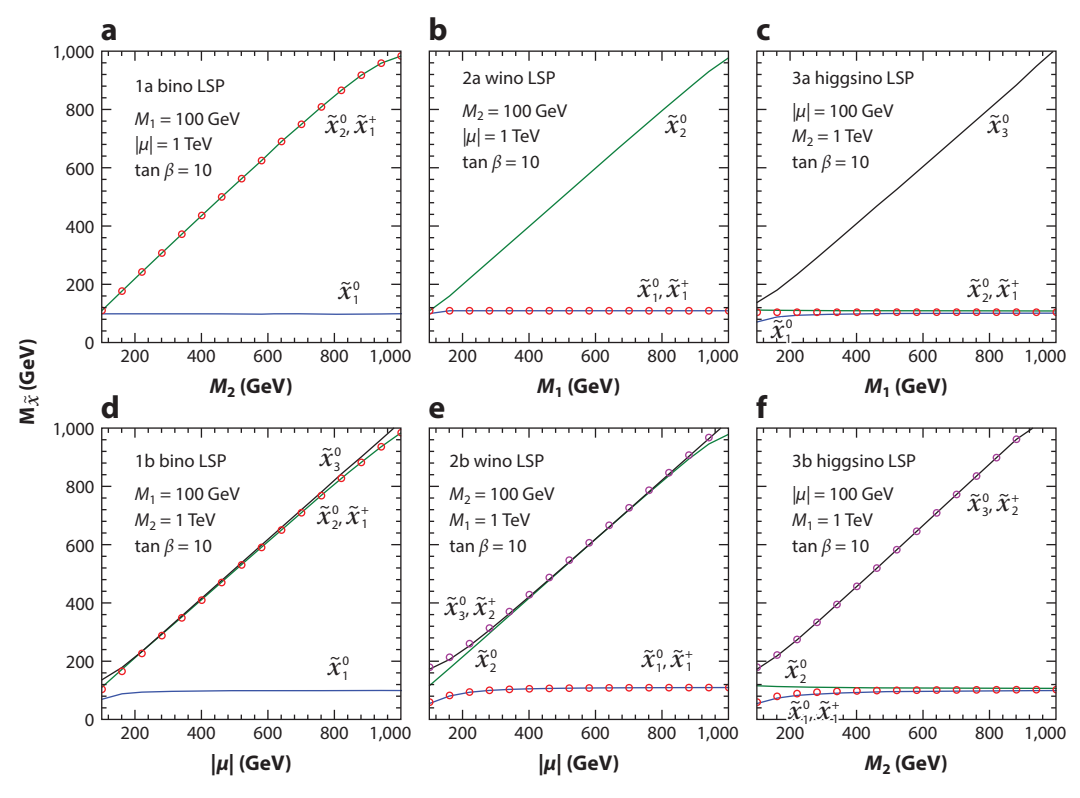


Figure 1

Electroweakino masses (y axes) of the LSP and NLSP states versus the NLSP mass parameters (x axes) for the three scenarios described in Section 2. Solid curves indicate neutralino states, and circles indicate chargino states. The LSP mass parameter is set as 100 GeV, the heaviest mass parameter is set as 1 TeV, and $\tan \beta = 10$.

For Scenario 1a, we focus on the bino–wino mixing, and the higgsino can be decoupled by taking $|\mu| \gg M_1, M_2$. The effective neutralino mass matrix can be expressed as

$$M = \begin{pmatrix} M_1 & 0 \\ 0 & M_2 \end{pmatrix} - s_{2\beta} \frac{M_Z^2}{\mu} \begin{pmatrix} s_W^2 & -s_W c_W \\ -s_W c_W & c_W^2 \end{pmatrix} + \mathcal{O}\left(\frac{M_Z^3}{\mu^2}\right).$$
 6.

The mixing occurs only through the mixture of higgsino states at the order of $\mathcal{O}(M_Z^3/\mu)$. The mass splitting between wino-like NLSPs $\tilde{\chi}_1^{\pm}$ and $\tilde{\chi}_2^0$ is generated at the order of $\mathcal{O}(M_Z^3/\mu^2)$ or at one-loop level. For Scenario 1b, we focus on the bino-higgsino mixing, and the wino states can be decoupled by taking $M_2 \gg M_1$, μ . The effective neutralino mass matrix in the basis $\tilde{B}, \tilde{H}_{1,2}^0 \equiv (\tilde{H}_u^0 \mp \tilde{H}_d^0)/\sqrt{2}$ is

$$M = \begin{pmatrix} M_1 & -\frac{s_{\beta} + c_{\beta}}{\sqrt{2}} s_W M_Z & \frac{s_{\beta} - c_{\beta}}{\sqrt{2}} s_W M_Z \\ -\frac{s_{\beta} + c_{\beta}}{\sqrt{2}} s_W M_Z & \mu & 0 \\ \frac{s_{\beta} - c_{\beta}}{\sqrt{2}} s_W M_Z & 0 & -\mu \end{pmatrix} - \frac{M_W^2}{2M_2} \begin{pmatrix} 0 & 0 & 0 \\ 0 & 1 + s_{2\beta} & c_{2\beta} \\ 0 & c_{2\beta} & 1 - s_{2\beta} \end{pmatrix} + \mathcal{O}\left(\frac{M_W^3}{M_2^2}\right).$$

Figure 1 illustrates the electroweakino masses of the LSP states and NLSP states versus the NLSP mass parameters. **Figure 1***a* shows electroweakino mass versus M_2 for Scenario 1a, and **Figure 1***d* shows electroweakino mass versus μ for Scenario 1b. It can be seen (e.g., in Scenario 1b) that a mass splitting among the higgsino multiplet is appreciable only when $\mu \sim M_1$ or $\mu \sim M_2$.

2.2. Scenario 2: Wino Lightest Supersymmetric Particles

We next consider the scenario in which M_2 is lower than the other two parameters, M_1 and μ . This scenario with wino-like LSPs is favored by the anomaly mediation of SUSY breaking (AMSB) model (47–49). The dimension 4 effective Lagrangian describing the interaction of the wino triplet (\tilde{W}) with the SM electroweak gauge bosons is given by

$$\mathcal{L}_{V\tilde{W}\tilde{W}} \supseteq -g\left(\overline{\tilde{W}^{0}}\gamma^{\mu}\tilde{W}^{+}W_{\mu}^{-} + \text{h.c.}\right) + g\overline{\tilde{W}^{-}}\gamma^{\mu}\tilde{W}^{-}(\cos\theta_{W}Z_{\mu} + \sin\theta_{W}A_{\mu}),$$
 7.

where g is the SU(2)_L gauge coupling. In the absence of large corrections from couplings with the fermion and sfermion sectors of the MSSM, these gauge interactions induce a mass splitting between the charged and neutral winos ($\delta m_{\tilde{W}}$), which at the two-loop order can be parameterized as follows (50):

$$\frac{\delta m_{\tilde{W}}}{1 \text{ MeV}} = 164.108 + 0.742735 \left(\log \frac{m_{\tilde{\chi}_0}}{1 \text{ TeV}} \right) - 0.540255 \left(\log \frac{m_{\tilde{\chi}_0}}{1 \text{ TeV}} \right)^2$$

$$+ 0.404201 \left(\log \frac{m_{\tilde{\chi}_0}}{1 \text{ TeV}} \right)^3 - 0.181509 \left(\log \frac{m_{\tilde{\chi}_0}}{1 \text{ TeV}} \right)^4,$$
8.

where $m_{\tilde{\chi}_0}$ is the neutral wino mass. The mass difference has a weak dependence on $m_{\tilde{\chi}_0}$ and is approximately 164 MeV for heavy $m_{\tilde{\chi}_0}$. The corresponding decay lifetime of the charged wino to a neutral wino and a charged pion is given in terms of the $c\tau$ value by Reference 50:

$$c au \simeq 3.1 \text{ cm} \left[\left(\frac{\delta m_{\tilde{W}}}{164 \text{ MeV}} \right)^3 \sqrt{1 - \frac{m_{\pi}^2}{\delta m_{\tilde{W}}^2}} \right]^{-1},$$
 9.

where m_{π} is the charged pion mass. We have normalized the mass difference to 164 MeV, which is the mass splitting in the limit $m_{\tilde{\chi}_0} \gg M_W$.

Beyond the pure wino situation, we consider two distinctive scenarios for the lower-lying state mixing:

Scenario 2a
$$M_2 < M_1 < \mu : \tilde{\chi}_1^{\pm}, \tilde{\chi}_1^0$$
 wino-like LSPs; $\tilde{\chi}_2^0$ bino-like NLSP 10.

Scenario 2b
$$M_2 < \mu < M_1: \ \tilde{\chi}_1^{\pm}, \tilde{\chi}_1^{0}$$
 wino-like LSPs; $\tilde{\chi}_2^{\pm}, \tilde{\chi}_{2,3}^{0}$ higgsino-like NLSPs 11.

As for the wino-higgsino mixing in Scenario 2b, the bino can be decoupled by taking $M_1 \gg M_2$ and μ , and the effective neutralino mass matrix can be effectively described by

$$M = \begin{pmatrix} M_1 & \frac{s_{\beta} + \epsilon_{\beta}}{\sqrt{2}} c_W M_Z - \frac{s_{\beta} - \epsilon_{\beta}}{\sqrt{2}} c_W M_Z \\ \frac{s_{\beta} + \epsilon_{\beta}}{\sqrt{2}} c_W M_Z & \mu & 0 \\ -\frac{s_{\beta} - \epsilon_{\beta}}{\sqrt{2}} c_W M_Z & 0 & -\mu \end{pmatrix} - \frac{M_Z^2 s_W^2}{2M_1} \begin{pmatrix} 0 & 0 & 0 \\ 0 & 1 + s_{2\beta} & c_{2\beta} \\ 0 & c_{2\beta} & 1 - s_{2\beta} \end{pmatrix} + \mathcal{O}\left(\frac{M_Z^3}{M_1^2}\right).$$

Figure 1 shows the physical LSP and NLSP masses for Scenario 2a versus M_1 (**Figure 1***b*) and for Scenario 2b versus $|\mu|$ (**Figure 1***e*).

2.3. Scenario 3: Higgsino Lightest Supersymmetric Particles

For μ to be lower than the other two parameters, M_1 and M_2 , the higgsino multiplet is essentially the LSP. This scenario is favored in the argument for natural SUSY (32–34). The effective interaction Lagrangian at dimension 4 for charged (\tilde{H}^{\pm}) and neutral (\tilde{H}^0) Dirac higgsinos with the SM

electroweak gauge bosons is given by

$$\mathcal{L}_{V\chi H\chi H} \supseteq -\frac{g}{\sqrt{2}} \left(\tilde{H}^{0} \gamma^{\mu} \tilde{H}^{-} W_{\mu}^{+} + \text{h.c.} \right) + g \overline{\tilde{H}^{-}} \gamma^{\mu} \tilde{H}^{-} \left(\frac{1/2 - s_{W}^{2}}{c_{W}} Z_{\mu} + s_{W} A_{\mu} \right)$$

$$-\frac{g}{2c_{W}} \overline{\tilde{H}^{0}} \gamma^{\mu} \tilde{H}^{0} Z_{\mu}, \qquad 12.$$

where s_W indicates $\sin \theta_W$ and c_W indicates $\cos \theta_W$. Note that the last term vanishes for the Majorana higgsino. The above interactions induce a one-loop mass splitting between the charged and neutral states $(\delta m_{\tilde{H}})$, which can be written as

$$\delta m_{\tilde{H}} = \frac{g^2}{16\pi^2} m_{\tilde{H}} \sin^2 \theta_W f\left(\frac{M_Z}{m_{\tilde{H}}}\right), \ f(r) = r^4 \ln r - r^2 - r\sqrt{r^2 - 4}(r^2 + 2) \ln \frac{\sqrt{r^2 - 4} + r}{2}.$$

The corresponding decay lifetime of the charged higgsino to a charged pion can be parameterized in terms of the $c\tau$ value as (51)

$$c\tau \simeq 0.7 \text{ cm} \times \left[\left(\frac{\delta m_{\tilde{H}}}{340 \text{ MeV}} \right)^3 \sqrt{1 - \frac{m_{\pi}^2}{\delta m_{\tilde{H}}^2}} \right]^{-1}.$$
 13.

As can be seen from Equations 9 and 13, for typical values of the mass splitting between the charged and neutral states, the charged wino has a considerably larger decay length compared with the charged higgsino. This makes the searches for long-lived particles potentially more favorable for winos than for higgsinos.

Depending on which is the lighter of M_1 and M_2 , there are two scenarios for the lower-lying state mixing:

Scenario 3a
$$\mu < M_1 < M_2$$
: $\tilde{\chi}_1^{\pm}$, $\tilde{\chi}_{1,2}^{0}$ higgsino-like LSPs; $\tilde{\chi}_3^{0}$ bino-like NLSP

Scenario 3b
$$\mu < M_2 < M_1: \tilde{\chi}_1^{\pm}, \tilde{\chi}_{1,2}^{0}$$
 higgsino-like LSPs; $\tilde{\chi}_2^{\pm}, \tilde{\chi}_3^{0}$ wino-like NLSPs 15.

The physical masses of the LSPs and NLSPs are shown in **Figure 1**c for Scenario 3a versus M_1 and in **Figure 1**f for Scenario 3b versus M_2 with $\mu = 100$ GeV. Relatively large mixing occurs for smaller values of M_1 and M_2 (i.e., <300 GeV) when close to μ .

2.4. Simplified Model and Phenomenological Minimal Supersymmetric Standard Model

The SUSY partner mass spectrum crucially depends on the SUSY breaking scale and the mechanism to mediate the effects to the SM sector (52). Well-formulated scenarios include mSUGRA (40–46), which predicts a bino-like LSP with $M_1:M_2:M_3\approx 1:2:7$; minimal gauge mediation (GMSB), which typically yields a very light gravitino LSP (53–59); AMSB (47–49), which prefers a wino-like LSP with $M_2:M_1:M_3\approx 1:3:8$; and natural SUSY, which argues for a higgsino LSP with $\mu\sim\mathcal{O}(M_Z)$ (32–34). However, those minimal and predictive scenarios are too restrictive and are highly constrained by the current experimental observations (such as the direct searches at the LHC and the 125-GeV SM-like Higgs boson) for mSUGRA and GMSB (60–64) and by astronomical constraints for AMSB (65). It is therefore prudent to consider the less restrictive situation in which the soft-SUSY breaking masses and $|\mu|$ are treated as free parameters as outlined in the previous sections, in accordance with the "simplified model" defined by an effective Lagrangian

(66, 67). In the simplified models under the current consideration, the nature of the sparticles is set to pure states, while the masses and decay branching fractions are set to chosen values. In the phenomenological MSSM (pMSSM) (68), the masses, cross sections, and branching fractions are instead derived from the M_1 , M_2 , and μ values, which are assumed to be free parameters. The pMSSM therefore captures the complex pattern of the electroweakino masses and decay channels realized when the electroweakinos have sizable mixing among the bino, winos, and higgsinos.

3. DARK MATTER RELIC DENSITY AND DIRECT DETECTION CONSTRAINTS

While there is stunning evidence for its existence in the Universe in the form of cold nonbaryonic matter, and it provides a clear argument for BSM physics, there is no particular indication of what form DM actually takes. This is because, so far, DM manifests itself only through gravitational interactions. However, there is a strong theoretical preference for DM to consist of WIMPs near the electroweak scale because this scenario yields the correct ballpark of the relic abundance and the possible connection to the next scale of BSM physics. Among the options of viable cold DM candidates, the lightest electroweakino (LSP) in *R* parity–conserving SUSY theories provides a natural candidate for DM (27). In this section, we discuss the DM connection of electroweakinos.

3.1. Relic Density

The paradigm of thermal decoupling, which is based on applications to cosmology of statistical mechanics and particle and nuclear physics, is enormously successful at making detailed predictions for observables in the early Universe, including the abundance of light elements and the cosmic microwave background. In this spirit, the relic abundance of DM particles is set by their annihilation cross section to the SM particles $\sigma \propto g_{\rm eff}^4/M_{\rm DM}^2$ in the early Universe (69–71):

$$\Omega b^2 = 0.11 \times \left(\frac{2.2 \times 10^{-26} \text{ cm}^3 \text{ s}^{-1}}{\langle \sigma v \rangle_{\text{freeze}}} \right).$$
 16.

To avoid overclosure of the Universe, today's relic abundance $\Omega b^2 \sim 0.11$ translates to a bound on the DM mass as

$$M_{\rm DM} < 1.8~{\rm TeV}\left(\frac{g_{\rm eff}^2}{0.3}\right).$$
 17.

The natural presence of the TeV scale and the electroweak coupling strength leads to the notion of the WIMP miracle (27). Because of the efficient annihilation to SM particles in the early Universe, the wino-like and higgsino-like DM will typically be underabundant. However, a heavier wino DM or higgsino DM with a mass of 3.1 or 1.1 TeV, respectively, could fully account for the thermal relic density (65, 72) and provides a well-motivated target for collider searches.

Beyond the generic considerations described above, acceptable WIMP DM relic density may be achievable by tuning the mass parameters. Widely explored examples include the coannihilation mechanisms (73–76), in which the LSP mass is close to that of another sparticle so that they effectively annihilate into SM particles to reach a desirable relic abundance, such as squark coannihilation (77–79), slepton coannihilation (80–83), and bino–wino coannihilation (84). These mechanisms all lead to a rich and characteristic phenomenology at colliders because of the coexistence of light SUSY states. A funnel annihilation is another example (85, 86), in which the mass of the *CP*-odd Higgs boson is tuned to be $m_A \approx 2m_{\tilde{\chi}_1^0}$ for effective LSP annihilation. In this case, it is possible to make electroweakinos as heavy as $\mathcal{O}(10 \text{ TeV})$, which is still consistent with the

bound of thermal relic abundance (87). For such a heavy WIMP DM mass, indirect detections of the relic DM annihilation by astrophysical observations may achieve better sensitivities (65, 88).

3.2. Direct Detection

If the halo of the Milky Way consists of WIMPs, then a WIMP flux of about 10² to 10³ cm⁻² s⁻¹ must pass through the Earth's surface. A convincing proof of the WIMP hypothesis would be the direct detection of these particles—for example, by observation of nuclear recoil after WIMP-nucleus elastic scattering on a nuclear target in the underground experiments.

For electroweakinos as the DM candidate, the neutralino LSP couples to the spin of the nucleus via the axial vector interaction $Z\tilde{\chi}_1^0\tilde{\chi}_1^0$ [spin dependent (SD)] and is independent of the nucleus spin via the scalar interaction $H\tilde{\chi}_1^0\tilde{\chi}_1^0$ [spin independent (SI)]. The scattering cross section on a heavy nuclear target with atomic number A will be proportional to A^2 in SI interactions because of the coherent effect of the nucleons. DM direct detections are thus more sensitive to the SI interactions. However, the SD interactions may still be significant because of the stronger gauge interactions via the Z exchange.

3.2.1. Current bounds on weakly interacting massive particle–nucleon cross sections from direct detection. At present, direct detection searches (89) have excluded SI DM-nucleon cross sections as low as 10^{-46} cm² (see Figure 2) and SD cross sections as low as 10^{-41} cm². In Figure 2, the leading results in the 5-GeV range and below come from the DarkSide-50 liquid Ar time-projection chamber (TPC) low-mass search and from cryogenic solid-state detectors, while the leading results for higher masses have been obtained using cryogenic noble liquids—a method pioneered in the last decade by the XENON program at LNGS. Projected sensitivities of near-future direct detection DM searches are shown in Figure 2. Three midterm searches using Xe TPCs (LZ, PANDA, and XENON-nT) all aim to reach 10^{-48} cm² scale sensitivity at a DM mass of 30 GeV. The DarkSide-20k experiment is expected to reach the 10^{-47} cm² scale at 1 TeV. Long-term future searches using Xe (DARWIN) and Ar (ARGO) are projected to reach beyond 10^{-48} cm² in the next decade. For SD interactions, near-term future experiments using Xe and CF₃ targets are projected to reach sensitivity to 10^{-42} cm² WIMP-neutron and WIMP-proton cross sections at 50 GeV. At low mass (around 1–10 GeV), solid-state experiments (e.g., SuperCDMS) expect to achieve a 10^{-42} cm² cross-section reach on a 5-year time scale.

3.2.2. Theory parameter space and complementarity of direct detection and collider searches. The null results from the DM direct detection have put stringent limits on the DM-nucleon scattering cross sections, thus challenging the WIMP miracle paradigm. Yet, caution needs to be taken when interpreting the current DM direct detection results because the DM interactions with the SM particles may be subtle (see **Figure 2**).

It has been realized that some blind spots exist in the SUSY neutralino parameter space where the direct detection cross section is highly suppressed because of subtle cancellation of the couplings (93). The direct detection rate of the neutralino DM in underground laboratories is sensitive to the couplings of $H\tilde{\chi}_1^0\tilde{\chi}_1^0$ and $Z\tilde{\chi}_1^0\tilde{\chi}_1^0$, which are governed by the components of the $\tilde{\chi}_1^0$ admixture. If the theory parameters satisfy certain conditions, the $H\tilde{\chi}_1^0\tilde{\chi}_1^0$ coupling vanishes (93) and thus leads to a vanishing SI cross section. Analogously, the $Z\tilde{\chi}_1^0\tilde{\chi}_1^0$ coupling also can be vanishingly small, which would lead to a highly suppressed SD cross section (94). If the heavy CP-even Higgs boson in the MSSM is not decoupled, it can also destructively interfere with the scattering via the light CP-even Higgs boson, leading to a new SI blind spot (79, 95, 96).

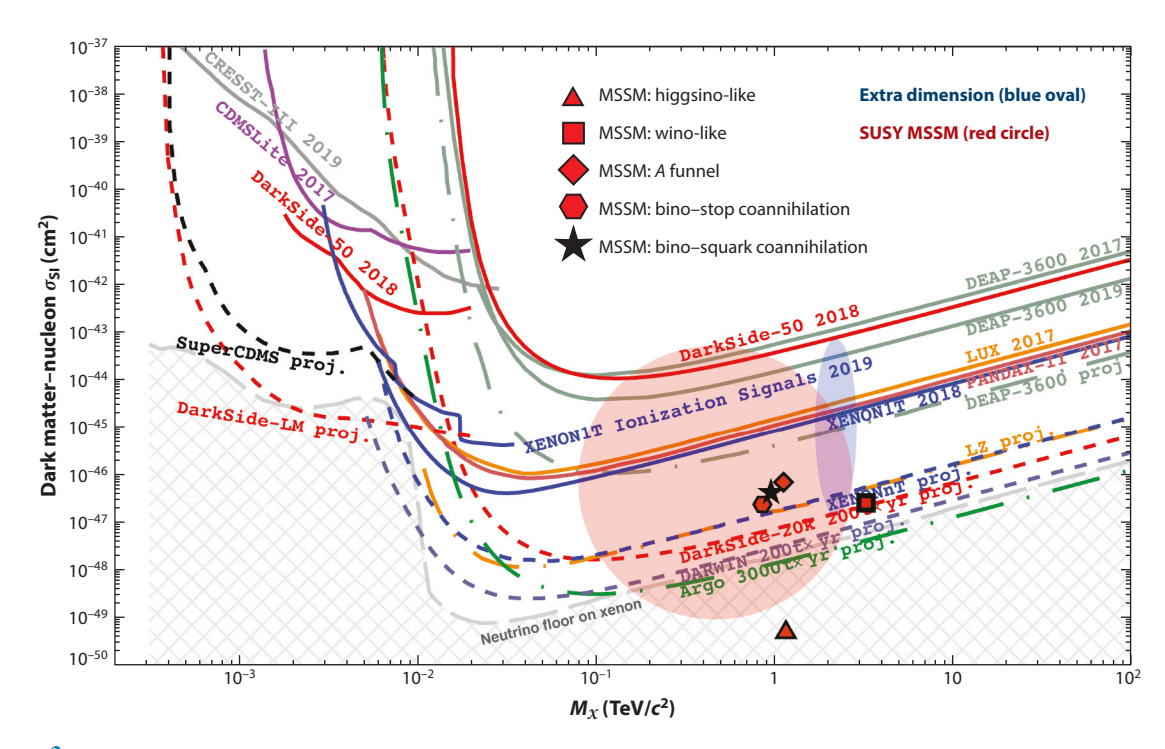


Figure 2

The 90% confidence level exclusion limits from DM direct detection (89) on the SI cross section versus the DM mass (solid and dashed lines) and some representative predictions in SUSY models (90–92). Theoretical predictions are included for the general MSSM (large red circle) and the Kaluza–Klein universal extradimensional model (blue oval). Also shown are special cases of loop-suppressed wino-like (red square, Scenario 2) and higgsino-like (red triangle, Scenario 3) DM. Of particular interest are the cases that yield the correct relic abundance via bino–stop coannihilation (red bexagon), bino–squark coannihilation (black star), and the CP-odd Higgs boson funnel (red diamond). Figure adapted from Reference 89 (CC BY 4.0).

It has been shown (97) that the blind spots still exist after the one-loop corrections are included, with their exact locations slightly shifted at an order of $\mathcal{O}(1\%)$. In some regions, the one-loop corrections to the SI cross section can reach values up to a few times 10^{-47} cm², which will be detectable at future multiton-scale liquid Xe experiments.

While the above arguments clearly indicate the need to improve the detection sensitivity for discovery, complementary searches at colliders are necessary. Indeed, SUSY searches at the LHC will substantially extend the coverage of the DM direct detections to the TeV mass region regardless of the direct detection blind-spot scenarios (94). If a signal is observed either in the DM direct detection or at the LHC experiments, determining its mass scale and coupling is of ultimate importance. Only with measurements from both types of experiments can one reach a full characterization of SUSY DM.

4. COLLIDER SEARCHES

4.1. Production at e^+e^- Colliders

Electroweakinos can be pair produced by electroweak processes at colliders. At e^+e^- colliders, assuming decoupling of the sleptons, the leading production processes are through s-channel

exchange of γ and Z bosons:

$$e^+e^- \to \gamma^*/Z^* \to \tilde{\chi}_i^+ \tilde{\chi}_i^-, \quad \tilde{\chi}_i^0 \tilde{\chi}_i^0,$$
 18.

where i, j = 1...4 for neutralinos and i, j = 1...2 for charginos. The pair production cross sections scale like

$$\sigma pprox rac{\pi \alpha^2 Q_{ij}^2}{s} eta,$$
 19.

where s is the center-of-mass energy squared, $\beta = \sqrt{1 - (m_i + m_j)^2/s}$, and Q_{ij} indicates some gauge charges (98, 99). The pair production rate can reach 1–100 fb at $\sqrt{s} = 1,000$ GeV (100, 101).

The signal observation through the decay products of the electroweakinos in the SM particles would be straightforward because of the clean experimental environment in e^+e^- collisions (100). In cases in which the final states contain neither reconstructed tracks nor significant energy deposits from electroweakino decays, the searches rely on the initial-state radiation (ISR) (102–107),

$$e^+e^- \to \tilde{\chi}_i^+ \tilde{\chi}_i^- \gamma, \quad \tilde{\chi}_i^0 \tilde{\chi}_i^0 \gamma,$$
 20.

to identify an isolated hard photon plus large recoil missing mass $m_{\text{recoil}}^2 = (p_{e^+} + p_{e^-} - p_{\gamma})^2$. The sensitivity reach is essentially kinematically limited, with $M_1, M_2, \mu \sim \sqrt{s}/2$. For further detailed discussions, readers are referred to general reports such as Reference 108.

Through the precision measurement of the Z boson's invisible width, the LEP experiments placed a lower bound on the mass of $\tilde{\chi}_1^0$ at 45.5 GeV under the assumption of a significant $\tilde{\chi}_1^0$ -Z coupling (109). However, massless neutralinos are allowed in scenarios with small couplings (110). By scanning particle production at the threshold, the LEP experiments also probed for the existence of charginos in a quasi-model-independent fashion. Results from the searches in the LEP data led to the model-independent bound on the chargino mass,

$$m_{\tilde{\chi}^{\pm}} > 103.5 \text{ GeV if } \Delta M(\tilde{\chi}_{1}^{\pm}, \tilde{\chi}_{1}^{0}) \ge 3 \text{ GeV}.$$
 21.

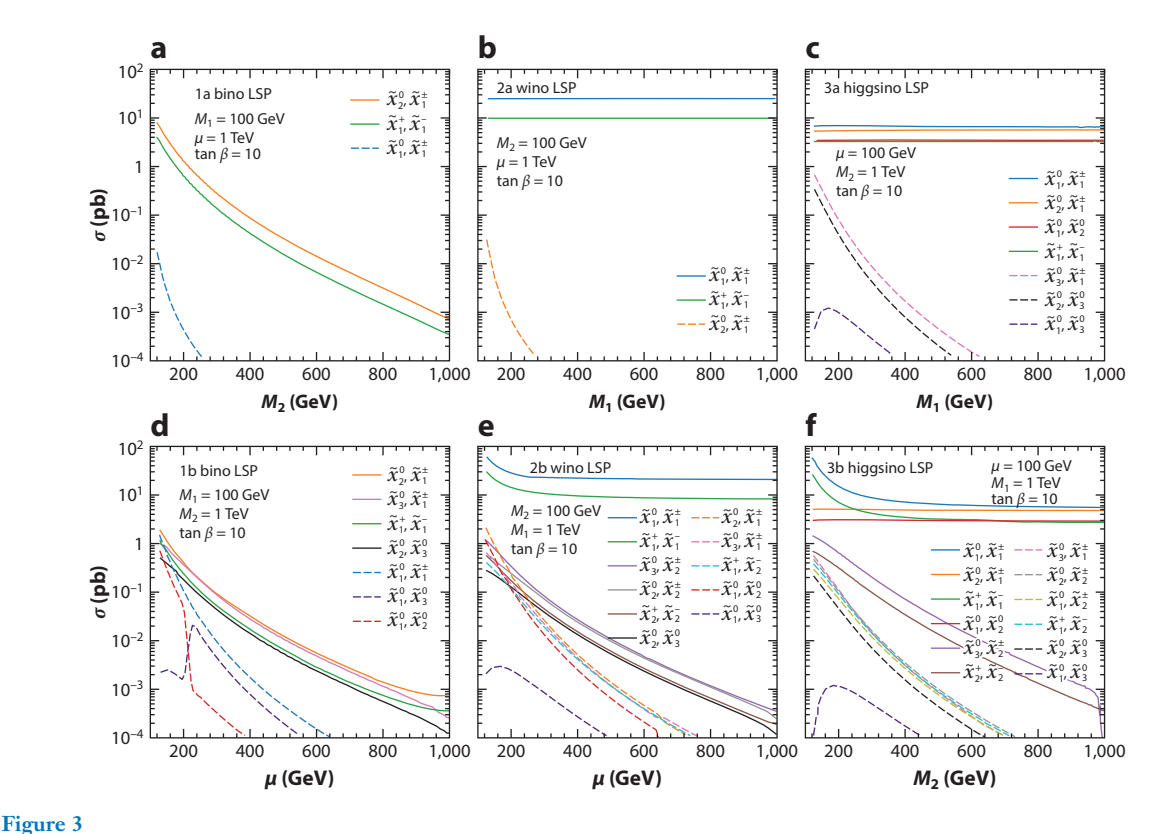
The bound is reduced to 92.4 GeV for smaller ΔM values (111). We take 100 GeV as our benchmark LSP mass for subsequent illustrations in this review.

4.2. Production at Hadron Colliders and Next Lightest Supersymmetric Particle Decays

Assuming decoupling of the squarks, the leading contribution at hadron colliders is from the schannel Drell-Yan (DY) processes with γ , W, and Z exchanges,

$$pp \to \tilde{\chi}_i^+ \tilde{\chi}_i^- X, \quad \tilde{\chi}_i^{\pm} \tilde{\chi}_i^0 X, \quad \tilde{\chi}_i^0 \tilde{\chi}_i^0 X,$$
 22.

where X generically denotes the hadronic remnants associated with the protons. Dominant processes are typically those that involve two wino-like or two higgsino-like states because their couplings to W, Z, and γ are unsuppressed. Electroweakino pair production via W exchange has the largest cross section because of large SU(2)_L coupling. **Figure 3** plots the pair production cross sections for electroweakinos via the DY processes at the LHC at $\sqrt{s} = 14$ TeV, following the three representative scenarios described in Section 2.



Electroweakino production cross sections at the LHC at $\sqrt{s} = 14$ TeV (112) versus the NLSP mass parameter for the three scenarios described in Section 2. The LSP mass parameter is set as 100 GeV, the heaviest mass parameter is set as 1 TeV, and $\tan \beta = 10$.

4.2.1. Scenario 1: bino lightest supersymmetric particle. Scenario 1a is characterized by a bino-like LSP and three wino-like NLSPs. With the unsuppressed SU(2)_L couplings, the leading production channels are the triplet wino-like NLSPs,

$$pp \to \tilde{\chi}_1^{\pm} \tilde{\chi}_2^0 X, \ \tilde{\chi}_1^{\pm} \tilde{\chi}_1^{\mp} X.$$
 23.

As shown in **Figure 3**a, their cross sections can be on the order of 1 pb to 1 fb for $M_2 \sim 200$ to 800 GeV. Although kinematically favored, the bino-like LSP production of $\tilde{\chi}_1^0 \tilde{\chi}_1^{\pm}$ and $\tilde{\chi}_1^0 \tilde{\chi}_2^0$ is highly suppressed by the bino-wino mixing. The wino NLSPs decay to the LSP $\tilde{\chi}_1^0$ plus their SM partners through the mixture of higgsino states. Therefore, the partial decay widths are scaled with a suppression factor $\mathcal{O}(M_Z/\mu)$. The branching fraction BF($\tilde{\chi}_1^{\pm} \to \tilde{\chi}_1^0 W^{\pm}$) is 100%. For $\tilde{\chi}_2^0$ decay, there are two competing channels,

$$\tilde{\chi}_2^0 \rightarrow Z \tilde{\chi}_1^0, H \tilde{\chi}_1^0,$$
 24.

once such channels are kinematically accessible. Those decay branching fractions are shown in **Figure 4a** versus M_2 . Once the $\chi_2^0 \to \chi_1^0 H$ channel is open, it quickly dominates for $\mu > 0$. In the case of $\mu < 0$, the branching fractions of Z and H modes are reversed. In particular, there is a dip in $\mathrm{BF}(\tilde{\chi}_2^0 \to \tilde{\chi}_1^0 H)$, as shown in **Figure 4a**, because the partial width is proportional to $(2\sin{(2\beta)} + M_2/\mu)$. Below the threshold for an on-shell Z, the branching fractions for various final states through an off-shell Z decay to the SM fermions, about 55% into light quarks, 15% into $b\bar{b}$, 20% into neutrinos, and 3.3% into each lepton flavor. For M_2 slightly above M_1 , the loop-induced

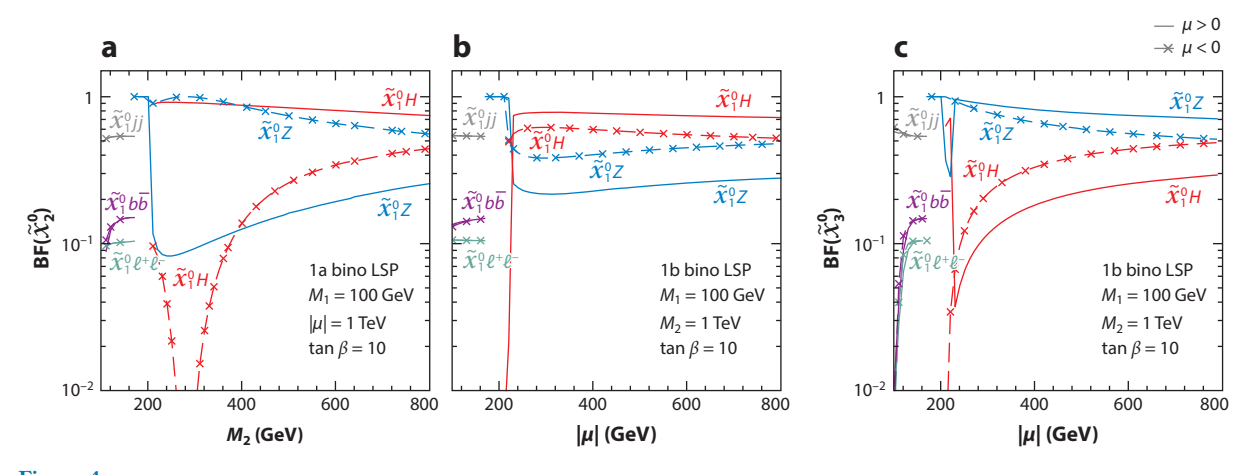


Figure 4

Decay branching fractions of (a) wino-like NLSPs in Scenario 1a and (b,c) higgsino-like NLSPs in Scenario 1b, as functions of the NLSP mass parameters. The LSP is chosen to be bino-like, with $M_1 = 100$ GeV. The heaviest mass parameter is set as 1 TeV, and $\beta = 10$.

radiative decay $\tilde{\chi}_2^0 \to \tilde{\chi}_1^0 \gamma$ becomes appreciable, although the final-state photon will be very soft, making its identification difficult.

Scenario 1b is characterized by a bino-like LSP and four higgsino-like NLSPs. The leading production channels are the higgsino-like NLSPs:

$$pp \to \tilde{\chi}_{1}^{\pm} \tilde{\chi}_{2}^{0} X, \quad \tilde{\chi}_{1}^{\pm} \tilde{\chi}_{3}^{0} X, \quad \tilde{\chi}_{1}^{+} \tilde{\chi}_{1}^{-} X, \quad \tilde{\chi}_{2}^{0} \tilde{\chi}_{3}^{0} X.$$
 25.

As shown in Figure 3d, their cross sections can be on the order of 500 to 1 fb for $\mu \sim 200$ to 800 GeV. Again, the bino-like LSP production of $\tilde{\chi}_1^0 \tilde{\chi}_1^{\pm}$, $\tilde{\chi}_1^0 \tilde{\chi}_2^{\pm}$, etc., is suppressed except when $M_1 \sim \mu$, in which case the mixing becomes substantial. The branching fraction BF($\tilde{\chi}_1^{\pm} \to \tilde{\chi}_1^0 W^{\pm}$) in Scenario 1b is again 100%. Figure 4 shows the decay branching fractions of $\tilde{\chi}_2^0$ (Figure 4b) and $\tilde{\chi}_3^0$ (**Figure 4***c*) through Z and H bosons versus μ for the higgsino NLSPs. For $\mu \gtrsim 250$ GeV, the decay pattern for $\tilde{\chi}_2^0$ is qualitatively similar to that of the light wino Scenario 1a with $\mu > 0$. The branching fraction of $\tilde{\chi}_2^0 \to \tilde{\chi}_1^0 H$ and $\tilde{\chi}_2^0 \to \tilde{\chi}_1^0 Z$ is about 75% and 25%, respectively, for $\mu =$ 500 GeV. The decays of $\tilde{\chi}_3^0$, however, are preferable to those of $\tilde{\chi}_1^0 Z$. The difference in the decay patterns of $\tilde{\chi}^0_2$ and $\tilde{\chi}^0_3$ is due to the different composition of $\tilde{\chi}^0_{2,3}$ as $\frac{1}{\sqrt{2}}(\tilde{H}^0_d \mp \tilde{H}^0_u)$. It should be noted that in **Figure 4c**, the branching fraction of $\tilde{\chi}_3^0 \to \tilde{\chi}_1^0 H$ shows a sudden drop around 230 GeV, coming from the level crossing of the two higgsino-like mass eigenstates. For $m_{\tilde{\chi}_1^0} - m_{\tilde{\chi}_1^0} < m_Z$, the off-shell decay of $\tilde{\chi}_2^0$ via Z^* again dominates, with the branching fraction of fermion final states similar to that of $\tilde{\chi}_2^0$ in Scenario 1a. The off-shell decays of $\tilde{\chi}_3^0$, in contrast, occur via both $\tilde{\chi}^0_3 \to \tilde{\chi}^\pm_1 W^*$ and $\tilde{\chi}^0_2 Z^*$. Even with the phase-space suppression when comparing the decay of $\tilde{\chi}_3^0$ directly down to $\tilde{\chi}_1^0$, the branching fractions for $\tilde{\chi}_3^0 \to \tilde{\chi}_1^{\pm} W^*$ could dominate over those of $\tilde{\chi}_3^0 \to \tilde{\chi}_1^0 Z^*$, as can be seen in **Figure 4c**, since the $\tilde{\chi}_3^0 \tilde{\chi}_1^{\pm} W$ coupling is unsuppressed, while $\tilde{\chi}_3^0 \tilde{\chi}_1^0 Z$ suffers from the small bino-higgsino mixing.

4.2.2. Scenario 2: wino lightest supersymmetric particles. For Scenario 2a with three wino-like LSPs and a bino-like NLSP $\tilde{\chi}_2^0$, the leading production channels are the wino-like triplet LSPs (similar to the scenario shown in Equation 23):

$$pp \to \tilde{\chi}_1^{\pm} \tilde{\chi}_1^0 X, \quad \tilde{\chi}_1^{+} \tilde{\chi}_1^{-} X.$$
 26.

The production cross sections at the LHC, which are shown in **Figure 3***b*, are about 10–20 pb for $M_2 = 100$ GeV. Although characterized by a large cross section, these processes bear a significant experimental challenge due to the small mass splitting of $m_{\tilde{\chi}_1^{\pm}} - m_{\tilde{\chi}_1^0}$, leading to $\tilde{\chi}_1^{\pm}$ decays into $\tilde{\chi}_1^0$ through the emission of pions, muons, or electrons. The final states will contain modest p_T^{miss} and very-low-transverse-momentum (p_T) tracks, requiring dedicated reconstruction techniques. We present the LHC searches in Section 4.3.

Scenario 2b is characterized by three wino-like LSPs and four higgsino-like NLSPs. The leading production channels are wino-like LSPs like the ones shown in Equation 26. The production cross sections at the LHC are shown in Figure 3e; the rate can be as large as 20 pb for $M_2 = 100$ GeV. From the observational aspect, similar to the situation of Scenario 2a, the compressed wino-like LSPs would be challenging to search for, as mentioned in the paragraph above and discussed in Section 4.3. In contrast, although subleading, the higgsino-like NLSP production is similar to that in Equation 25:

$$pp \to \tilde{\chi}_{2}^{\pm} \tilde{\chi}_{2}^{0} X, \quad \tilde{\chi}_{2}^{\pm} \tilde{\chi}_{3}^{0} X, \quad \tilde{\chi}_{2}^{+} \tilde{\chi}_{2}^{-} X, \quad \tilde{\chi}_{2}^{0} \tilde{\chi}_{3}^{0} X.$$
 27.

The cross sections are shown in **Figure** 3e and are quite sizable with the unsuppressed $SU(2)_L$ couplings, reaching the order of 500 to 1 fb for $\mu \sim 200$ to 800 GeV—similar to the case of Scenario 1b with higgsino-like NLSPs.

The decay patterns for the higgsino-like NLSPs are much richer. Generically, $\tilde{\chi}_{2,3}^0$ and $\tilde{\chi}_{2}^{\pm}$ decay to a W, Z, or H boson plus its corresponding LSP. The decay channels for the two NLSP neutralinos $\tilde{\chi}_{2,3}^0$ are

$$\tilde{\chi}_{2,3}^0 \to \tilde{\chi}_1^{\pm} W^{\mp}, \ \tilde{\chi}_1^0 Z, \ \tilde{\chi}_1^0 H.$$
 28.

Their decay branching fractions are shown in Figure 5a,b. They are Majorana fermions and decay to both $\tilde{\chi}_1^+W^-$ and $\tilde{\chi}_1^-W^+$ equally. Under the limit of $|\mu \pm M_2| \gg m_Z$, the following simplified relation holds for the partial decay widths (and decay branching fractions) of $\tilde{\chi}^0_{2,3}$:

$$\Gamma_{\tilde{\chi}_1^+W^-} = \Gamma_{\tilde{\chi}_1^-W^+} \approx \Gamma_{\tilde{\chi}_1^0Z} + \Gamma_{\tilde{\chi}_1^0H},$$
 29.

in accordance with the Goldstone boson equivalence theorem (113–116). The $\tilde{\chi}_2^0$ is more likely to decay to Z, whereas $\tilde{\chi}^0_3$ is more likely to decay to H for $\mu>0$. The sudden changes for the $\tilde{\chi}^0_1Z$

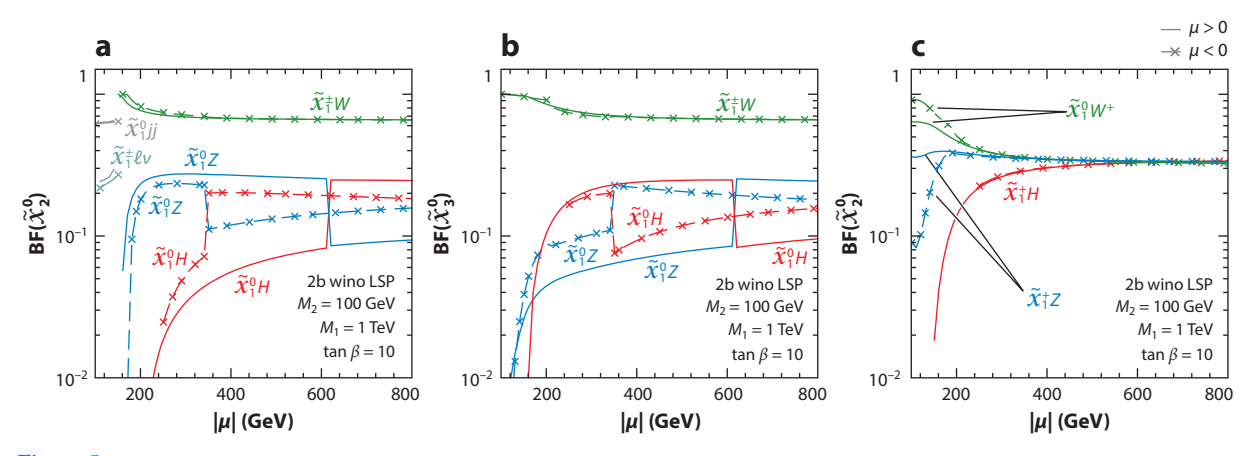


Figure 5

Decay branching fractions of higgsino-like NLSPs in Scenario 2b, as functions of the NLSP mass parameters. The LSP is chosen to be wino-like, with $M_2 = 100$ GeV. The heaviest mass parameter is set as 1 TeV, and $\tan \beta = 10$.

and $\tilde{\chi}_1^0 H$ channels shown in **Figure 5***a*,*b* are due to level crossing. For $\tilde{\chi}_2^{\pm}$, the dominant decay modes are

$$\tilde{\chi}_2^{\pm} \rightarrow \tilde{\chi}_1^0 W, \ \tilde{\chi}_1^{\pm} Z, \ \tilde{\chi}_1^{\pm} H.$$
 30.

Their decay branching fractions are shown in **Figure 5**c. Under the limit of $|\mu \pm M_2| \gg m_Z$, the ratios of the partial decay widths are roughly $\Gamma_{\tilde{\chi}_1^0 W}: \Gamma_{\tilde{\chi}_1^{\pm} Z}: \Gamma_{\tilde{\chi}_1^{\pm} H} \approx 1:1:1$, with small deviation caused by phase-space effects.

4.2.3. Scenario 3: higgsino lightest supersymmetric particles. For Scenario 3a with four higgsino-like LSPs and a bino-like NLSP $\tilde{\chi}_3^0$, the leading production channels are the LSP pairs (similar to the scenario shown in Equation 25):

$$pp \to \tilde{\chi}_1^{\pm} \tilde{\chi}_{1,2}^0 X, \quad \tilde{\chi}_1^{+} \tilde{\chi}_1^{-} X, \quad \tilde{\chi}_1^0 \tilde{\chi}_2^0 X.$$
 31.

The production cross sections at the LHC are shown in **Figure 3**c; the rate is about 5 pb for $\mu = 100$ GeV. As in Scenario 2, such channels are difficult to probe with conventional searches because of the compressed spectrum for the LSPs.

For Scenario 3b with four higgsino-like LSPs and three wino-like NLSPs, the leading production channels are the same as above for the higgsino-like LSP pairs in Equation 31. The production cross sections at the LHC are shown in **Figure 3**f; the rate can be as large as 5 pb for $\mu = 100$ GeV (similar to Scenario 3a). Again from the observational aspect, this situation is similar to those of Scenarios 2a, 2b, and 3a: The compressed LSPs would be challenging to search for, as mentioned above and discussed in Section 4.3. In contrast, the subleading channels for wino-like NLSP production as shown in Equation 23 come to the rescue. The cross sections, shown in **Figure 3**f; can be on the order of 1 pb to 1 fb for $M_2 \sim 200$ to 800 GeV (similar to the case of Scenario 1a).

The decay branching fractions for the NLSPs $\tilde{\chi}_2^{\pm}$ and $\tilde{\chi}_3^0$ in Scenario 3b are shown in **Figure** 6*a*,*b*. For $\tilde{\chi}_2^{\pm}$, the dominant decay modes are

$$\tilde{\chi}_{2}^{\pm} \to \tilde{\chi}_{1}^{0} W, \ \tilde{\chi}_{2}^{0} W, \ \tilde{\chi}_{1}^{\pm} Z, \ \tilde{\chi}_{1}^{\pm} H.$$
 32.

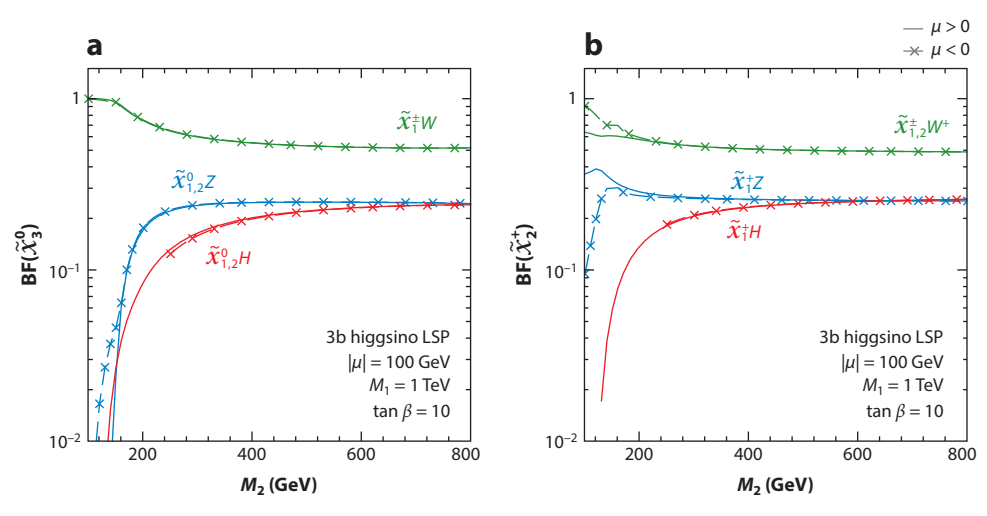


Figure 6

Decay branching fractions of wino-like NLSPs in Scenario 3b, as functions of the NLSP mass parameters. The LSP is chosen to be higgsino-like, with $|\mu| = 100$ GeV. The heaviest mass parameter is set as 1 TeV, and $\tan \beta = 10$.

Under the limit of $|M_2 \pm \mu| \gg m_Z$, the ratios of the partial decay widths are roughly $\Gamma_{\tilde{\chi}_1^0 W}$: $\Gamma_{\tilde{\chi}_2^0 W}: \Gamma_{\tilde{\chi}_1^\pm Z}: \Gamma_{\tilde{\chi}_1^\pm H} \approx 1:1:1:1$. Because of the LSP degeneracy of $\tilde{\chi}_1^0$ and $\tilde{\chi}_2^0$, the $\tilde{\chi}_1^0 W$ and $\tilde{\chi}_2^0 W$ final states would be indistinguishable experimentally. Combining these two channels, the branching fractions of $\tilde{\chi}_2^\pm$ to the W, Z, and H channels are roughly 51%, 26%, and 23%, respectively. In the limit of large M_2 , the branching fractions approach the asymptotic limit $\mathrm{BF}(\tilde{\chi}_2^\pm \to \tilde{\chi}_{1,2}^0 W) \approx 2\mathrm{BF}(\tilde{\chi}_2^\pm \to \tilde{\chi}_1^\pm H) \approx 2\mathrm{BF}(\tilde{\chi}_2^\pm \to \tilde{\chi}_1^\pm Z) \approx 50\%$. Combining the $\tilde{\chi}_1^0$ and $\tilde{\chi}_2^0$ final states, the branching fraction of the Z channel is almost the same as that of the H channel at very large $|M_2 \pm \mu| \gg m_Z$, which is about half of the branching fraction of the W final states. If kinematically accessible, the heavy Higgs bosons A^0 and $H^{0,\pm}$ may decay to a pair of electroweakinos with branching fractions of $\mathcal{O}(10{\text -}30\%)$, thereby providing new channels for the search (117).

Electroweakinos could also be produced via weak vector boson fusion processes (VBFs) (118–123):

$$qq' \rightarrow qq'\tilde{\chi}_i^+\tilde{\chi}_j^0, \ qq'\tilde{\chi}_i^+\tilde{\chi}_j^-, \ qq'\tilde{\chi}_i^0\tilde{\chi}_j^0.$$
 33.

The production rate for this mechanism is typically smaller than that of the DY processes by about two orders of magnitude, depending on the electroweakino masses. Thus, these channels do not contribute much to the inclusive signal (39). Nevertheless, the unique kinematics of the accompanying forward-backward jets makes the signal quite characteristic and the search very promising, as discussed in Section 4.3.3.

4.3. Searches at the ATLAS and CMS Experiments

From the beginning of the LHC era, direct searches for SUSY have represented one of the major science drivers of the ATLAS and CMS experiments. However, searches for electroweakinos have become the core of the SUSY program at the LHC since the discovery of a Higgs boson in 2012 and the collection of large data sets of proton–proton collisions at center-of-mass energies of 8 and 13 TeV. Besides the electroweakino mass scale that governs the production rate and decay kinematics, the other most characteristic parameter for the experimental searches is the mass difference between the decaying parent $\tilde{\chi}_{parent}$ and the daughter $\tilde{\chi}_{daughter}$, denoted by

$$\Delta M = m_{\tilde{\chi}_{\text{parent}}} - m_{\tilde{\chi}_{\text{daughter}}},$$

which determines the average transverse momentum of the daughter particles and thus dictates how candidate events are reconstructed by the experiments. For $\Delta M \gtrsim M_Z/M_W/m_H$, we consider this scenario as the noncompressed spectra, while $\Delta M \sim \mathcal{O}(1\text{--}10~\text{GeV})$ and $\Delta M \sim \mathcal{O}(100~\text{MeV})$ correspond to the compressed and nearly degenerate spectra, respectively.

The ATLAS and CMS Collaborations have designed comprehensive searches to target scenarios with noncompressed and compressed spectra (e.g., Scenario 1) with a bino-like LSP or to target scenarios such as 2b and 3b with lower-lying wino and higgsino states. The leading search channels address the generic DY pair production of the following:

- Charged and neutral electroweakinos with subsequent decays into $W \tilde{\chi}_1^0$ and $Z/H \tilde{\chi}_1^0$
- Two charged electroweakinos decaying into $W \tilde{\chi}_1^0 W \tilde{\chi}_1^0$

Results from these analyses are then interpreted in terms of the theory parameters associated with the scenarios described in Section 2, and thus they can be connected to the underlying theoretical models. Constraints can also be imposed on models that predict decays via other SUSY states (including, e.g., heavy Higgs bosons if kinematically allowed).

Nearly degenerate spectra arise in Scenarios 2 and 3 when the heavier multiplets are decoupled from the lightest one. As a result, the only accessible decays happen within the lightest wino-like

or higgsino-like multiplets, resulting in low-transverse-momentum decay products or long-lived electroweakinos. These scenarios require dedicated experimental techniques.

Searches for noncompressed scenarios are presented in Section 4.3.2, and those for compressed and nearly degenerate spectra are summarized in Sections 4.3.3 and 4.3.4, respectively.

4.3.1. Search methodology. The ATLAS and CMS Collaborations conduct searches for SUSY as blind analyses in that the signal regions (SRs) are defined by optimizing the expected sensitivity with respect to a selected model, which may be a realistic framework that assumes a specific SUSY breaking and mediation mechanism, or the phenomenological model referred to as the pMSSM, or a so-called simplified model. In the simplified models, the reinterpretation of the search results is presented in the parameter space defined by the masses of the charginos and neutralinos, under the assumption of pure states and 100% branching fraction into the final state of interest (unless specified). As presented in Section 2.4, the pMSSM space is instead defined by the μ , M_1 , and M_2 parameters that govern the electroweakinos' masses and composition and, thus, their production cross section and decay branching fractions.

Several SM processes lead to events similar to those expected from the electroweakinos' production and subsequent decays. The backgrounds due to the production of multijet, bosons plus jet, and top quark pairs are typically estimated using data-driven methods based on control regions (CRs), a subset of events with negligible signal contributions used to constrain the yields of SM processes. Backgrounds due to electroweak production of bosons and rare processes (e.g., diand triboson or Higgs boson production) are instead estimated using Monte Carlo simulated data with yields normalized to the state-of-the-art calculated cross sections. The background predictions obtained from a background-only fit of the CRs can be compared with the observed data in validation regions to verify the accuracy of the background modeling.

To extend the reach to the largest possible region of parameter space, candidate events are classified depending on the value of selected observables (e.g., $p_{\rm T}^{\rm miss}$); the observable's spectrum is binned into multiple SRs (up to hundreds). If the SM background expectations in all SRs are in agreement with the observed data within the estimated statistical and systematic uncertainties, the results from the search are interpreted as an upper limit on the SUSY production cross section. Likelihood fits are deployed assuming a background-only hypothesis, a model-independent signal plus background hypothesis, and a model-dependent signal plus background hypothesis. The likelihood incorporates information from all SRs and CRs defined in the analysis. This approach enables one to constrain the expected background to the yields observed in the data and reduce systematic uncertainties. The systematic uncertainties are considered in the fit as nuisance parameters and are constrained by selected distributions while taking into account correlations between signal and backgrounds. The upper limits on the number of SUSY events in each SR and the upper limits on the SUSY cross sections are computed at a 95% confidence level (CL) using the CL_s method (124–126). Model-independent upper limits are computed using Monte Carlo pseudoexperiments, and model-dependent upper limits are computed using asymptotic formulas (127).

4.3.2. Searches for noncompressed supersymmetric spectra. Searches for electroweakinos in noncompressed spectra are optimized for the s-channel production of mass-degenerate wino-like states $\tilde{\chi}_1^{\pm}$ and $\tilde{\chi}_2^0$. Their production cross sections at the LHC, shown in **Figure 3a**, **f**, are discussed as Scenarios 1a and 3b in Section 4.2.

Searches for $\tilde{\chi}_1^{\pm} \tilde{\chi}_2^0 \to W \tilde{\chi}_1^0 H \tilde{\chi}_1^0$ are typically carried out in final states with at least one lepton from the decay of the W boson in order to benefit from a reduction of the multijet background, while various decays of the Higgs boson are explored to maximize the sensitivity. The ATLAS Collaboration has recently completed a search based on 139 fb⁻¹ of proton–proton collision data

collected at $\sqrt{s} = 13$ TeV targeting Higgs boson decays into $b\bar{b}$ pairs (128). Signal-to-background discrimination is achieved by means of several mass observables:

- The invariant mass of the two-b-jet system³ required to be consistent with the Higgs boson mass
- The transverse mass $m_{\rm T} = \sqrt{2p_{\rm T}^{\rm miss}}p_{\rm T}(1-\cos\phi)$, where ϕ is the angular distance between the $\vec{p}_{\rm T}^{\rm miss}$ and the lepton in the transverse plane; when a particle decays into a charged and a neutral daughter, the $m_{\rm T}$ exhibits an endpoint at the value of the mother particle mass, and the $m_{\rm T}$ therefore helps to suppress events in which a W boson decays leptonically as $W \to \ell \nu$
- The invariant mass of the lepton and highest- p_T b jet, which exhibits an endpoint at $\sqrt{m^2(t) m^2(W)}$ in $t\bar{t}$ and single-top background events
- The cotransverse mass $m_{\rm CT} = \sqrt{2p_{\rm T}^{b_1}p_{\rm T}^{b_2}(1+\cos\Delta\phi_{bb})}$, where b_i (i=1,2) are the selected b jets and $\Delta\phi_{bb}$ is the azimuthal angle between them; the $m_{\rm CT}$ is adopted to suppress the $t\bar{t}$ background as well because it shows an endpoint at $(m^2(t)-m^2(W))/m(t)$

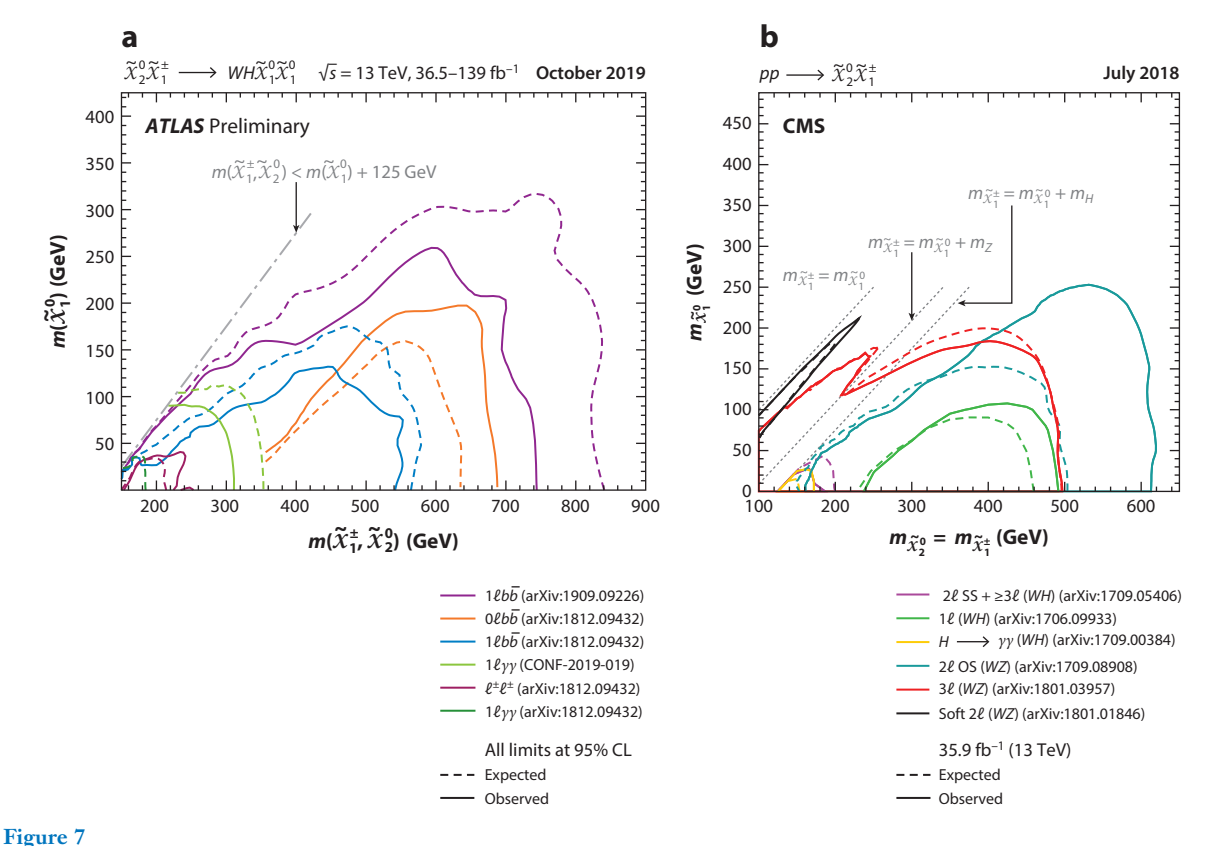
Degenerate wino-like $\tilde{\chi}_1^{\pm}$ and $\tilde{\chi}_2^0$ with masses up to 740 GeV are excluded for massless $\tilde{\chi}_1^0$. Results are presented in **Figure 7***a* along with those from a novel search in the fully hadronic mode $\tilde{\chi}_1^{\pm} \tilde{\chi}_2^0 \to WH \to q\bar{q}b\bar{b}$ (129), providing good sensitivity in the background-free region at large $\Delta M(\tilde{\chi}_2^0, \tilde{\chi}_1^0)$. The latest CMS searches for $\tilde{\chi}_1^{\pm} \tilde{\chi}_2^0 \to W \tilde{\chi}_1^0 H \tilde{\chi}_1^0$ are documented in References 130 and 131.

In scenarios in which the $Z\tilde{\chi}^0_2\tilde{\chi}^0_1$ coupling is significant, the search for $\tilde{\chi}^\pm_1\tilde{\chi}^0_2 \to W\tilde{\chi}^0_1Z\tilde{\chi}^0_1$ can probe a broad area of the $(m_{\tilde{\chi}_1^0}, m_{\tilde{\chi}_1^0})$ space thanks to the large width of the Z boson. If $\Delta M(\tilde{\chi}_2^0, \tilde{\chi}_1^0) \gg m_Z$, $\tilde{\chi}_1^{\pm} \tilde{\chi}_2^0$ production leads to final states with high- p_T leptons or jets from the gauge bosons' decay and significant p_T^{miss} . Both the ATLAS and CMS Collaborations have developed searches in events with two leptons from the Z decay and jets from the hadronic decay of the accompanying W boson (Z+i search). Selecting leptonic decay of the Z boson enables suppression of the multijet background, while exploration of the hadronic decays of the W boson maximizes signal acceptance. In the CMS Z+j search (132), the signal is separated from the remaining $t\bar{t}$ background by rejecting events with b jets and by means of the stransverse mass m_{T2} (133). The m_{T2} was originally defined to measure the mass of pair-produced particles, each decaying to a visible and an invisible particle, and can be exploited to identify the fully leptonic decays of top quarks $t\bar{t} \to W^+bW^-\bar{b} \to \ell^+\nu b\ell^-\nu \bar{b}$ as well as those from pair-produced W bosons. To maximize the reach, candidate events are categorized depending on the p_T^{miss} and the dijet invariant mass, which is expected to be consistent with the W boson mass in $\tilde{\chi}_1^{\pm} \tilde{\chi}_2^0 \to W \tilde{\chi}_1^0 Z \tilde{\chi}_1^0$ processes. Figure 7b shows that the Z+j CMS analysis excludes mass-degenerate wino-like $\tilde{\chi}_{\perp}^{\pm}$ and $\tilde{\chi}_{2}^{0}$ lighter than 610 GeV if the $\tilde{\chi}_{1}^{0}$ is massless. The ATLAS Z+j search has a similar reach (134).

In addition to searches for $\tilde{\chi}_1^{\pm} \tilde{\chi}_2^0$ production, the exploration of $\tilde{\chi}_1^{\pm}$ pair production followed by W-mediated decays also represents an avenue for discovery of scenarios with relatively large mass splittings. Because the $\tilde{\chi}_1^{\pm} \tilde{\chi}_1^{\mp}$ cross section is comparable to that of the $\tilde{\chi}_1^{\pm} \tilde{\chi}_2^0$ process, added sensitivity is achieved if the W^+W^- background is significantly suppressed. In Reference 135, the ATLAS Collaboration targets the challenging dilepton final state from $\tilde{\chi}_1^{\pm} \to W \tilde{\chi}_1^0 \to \ell \nu \tilde{\chi}_1^0$, categorizing events based on the m_{T2} , p_T^{miss} , and p_T^{miss} significance values. The analysis of 139 fb⁻¹ of data yields sensitivity to wino-like $\tilde{\chi}_1^{\pm}$ with masses up to 420 GeV if the $\tilde{\chi}_1^0$ is massless.

³Jets containing *b* hadrons are referred to as *b*-tagged or simply *b* jets.

⁴The $p_{\rm T}^{\rm miss}$ significance is computed on an event-by-event basis and evaluates the p-value that the observed $p_{\rm T}^{\rm miss}$ will be consistent with the null hypothesis of zero real $p_{\rm T}^{\rm miss}$ (136).



(a) The 95% CL exclusion limits on $\tilde{\chi}_1^{\pm} \tilde{\chi}_2^0$ production as a function of their masses and the $\tilde{\chi}_1^0$ mass. The $\tilde{\chi}_1^{\pm}$ and $\tilde{\chi}_2^0$ are assumed to decay into $\tilde{\chi}_1^0$ by emitting a W boson and an H boson, respectively. (b) The 95% CL exclusion limits set assuming various decays of the $\tilde{\chi}_2^0$, including decays via Z bosons. In both cases, the production cross section is for wino-like $\tilde{\chi}_1^{\pm}$ and $\tilde{\chi}_2^0$. Panel a adapted from https://atlas.web.cern.ch/Atlas/GROUPS/PHYSICS/PUBNOTES/ATL-PHYS-PUB-2020-013/ (CC BY 4.0). Panel b adapted from https://twiki.cern.ch/twiki/bin/view/CMSPublic/PhysicsResultsSUS#Run_2_Summary_plots_13_TeV.

Scenarios characterized by mass splittings closer to m_Z , in which the signal kinematics resembles that of the dominant WZ background, can be probed through the fully leptonic decays of the W and Z bosons from $\tilde{\chi}_1^{\pm} \tilde{\chi}_2^0 \to W \tilde{\chi}_1^0 Z \tilde{\chi}_1^0$. Such analyses, dubbed multilepton searches, typically request events with two leptons of same electric charge or three or more leptons. Selecting events with two same-charged leptons increases the acceptance to scenarios with small $\Delta M(\tilde{\chi}_2^0, \tilde{\chi}_1^0)$ in which one lepton happens to have a transverse momentum below the default threshold. The inclusive approach adopted by the multilepton CMS analysis (137) relies on splitting events with significant $p_{\rm T}^{\rm miss}$ into subcategories based on the number and flavor of leptons (electrons, muons, hadronically decaying taus) and topological and kinematical observables that include the following:

- the invariant mass of the two oppositely charged same-flavor leptons ($\ell^+\ell^-$), which allows identification and suppression of the SM WZ background;
- the $p_{T\ell^+\ell^-}$, which is sensitive to the production of a single resonance and thus can further discriminate events with and without a Z boson;

- the minimum m_T computed for each lepton in the event, a variable sensitive to the SM production of W bosons decaying into $\ell \nu$; and
- the m_{T2} exhibiting an endpoint at the W boson mass, which helps suppress the W^+W^- and $t\bar{t}$ SM backgrounds.

This analysis complements the sensitivity provided by the Z+j search, extending the reach to the bulk of the $(m_{\tilde{\chi}^0_2}, m_{\tilde{\chi}^0_1})$ space (see **Figure 7**). The CMS Collaboration also has implemented a statistical combination of the results from the two searches and extended the limit on the $\tilde{\chi}^{\pm}_1$ and $\tilde{\chi}^0_2$ mass by approximately 40 GeV for a massless $\tilde{\chi}^0_1$; this approach is sensitive to models with intermediate mass values that have not been probed by individual analyses (138). The multilepton ATLAS analyses are documented in References 134 and 139.

4.3.3. Searches for compressed supersymmetric spectra. Compressed spectra can emerge in Scenarios 1a and 1b as well as in Scenarios 2b and 3b. In these cases, the sensitivity of the classical searches described in Section 4.3.2 deteriorates significantly. These spectra can nevertheless be probed by exploring a subset of signal events with additional SM objects that enable the experiments to efficiently discriminate the signal from the background: events originating from the s-channel production of $\tilde{\chi}_i^{\pm}$ and $\tilde{\chi}_j^0$, in which an ISR jet boosts the sparticle system and increases the p_T^{miss} in the laboratory (ISR search), and events in which the sparticles are produced via VBF and are therefore accompanied by two jets from the protons' remnants located in opposite forward-backward regions of the detector (VBF search).

In the ISR analyses, the dominant multijet background is typically suppressed by reconstructing the two low- p_T same-flavor opposite-charged leptons from the $\tilde{\chi}^0_2 \to Z^* \tilde{\chi}^0_1$ decays and requiring their invariant mass to be compatible with the Z^* mass. To maximize the acceptance for scenarios with very small mass splittings, the ATLAS search (140) also includes an SR based on a lepton and an isolated track with p_T in the range of 1 to 5 GeV. This selection targets scenarios with a reconstructed $m_{\ell,tk}$ invariant mass between 0.5 and 5 GeV. In addition to optimized criteria based on the p_T^{miss} , m_T , b jet multiplicity, and subleading lepton p_T , signal-to-background discrimination in the ATLAS ISR search is obtained by exploiting the following:

- The $m_{\tau\tau}$ observable proposed in References 141–143, approximating the invariant mass of a τ pair where both τ s are boosted and decay leptonically; the $m_{\tau\tau}$ is deployed to reject events from $Z/Z^* \to \tau\tau$
- Two observables defined using the recursive jigsaw reconstruction technique⁵ (144)
- The ratio of p_T^{miss} to the scalar sum of the leptons' p_T ; this ratio is expected to be small in SM processes

The limits in the $(\tilde{\chi}_2^0, \Delta M)$ plane are obtained by fitting the dilepton invariant mass distribution under the assumption of either wino-like or higgsino-like electroweakinos. The results of the search carried out in 139 fb⁻¹ of data show that wino-like electroweakinos with masses up to 240 GeV are excluded if $m_{\tilde{\chi}_1^0} \times m_{\tilde{\chi}_2^0} > 0$ and $\Delta M(\tilde{\chi}_2^0, \tilde{\chi}_1^0) = 7$ GeV (**Figure 8a**). If the $\tilde{\chi}_1^{\pm}$ mass values are close to the LEP limit, mass splittings from 1.5 to 46 GeV are probed.

⁵In the jigsaw technique, the event is split into two hemispheres perpendicular to the thrust axis, approximating the direction of the recoil of the ISR jets against the sparticle pair: One hemisphere is expected to contain the decay products of the $\tilde{\chi}_1^{\pm}$ and $\tilde{\chi}_2^0$ (S system), while the opposite hemisphere is associated with the hadronic activity (ISR system). The ratio of $p_{\rm T}^{\rm miss}$ to the ISR system $p_{\rm T}$ is sensitive to the sparticle mass splitting, while the $m_{\rm T}$ of the S system can be used to suppress background events with W bosons thanks to its endpoint at the W mass.

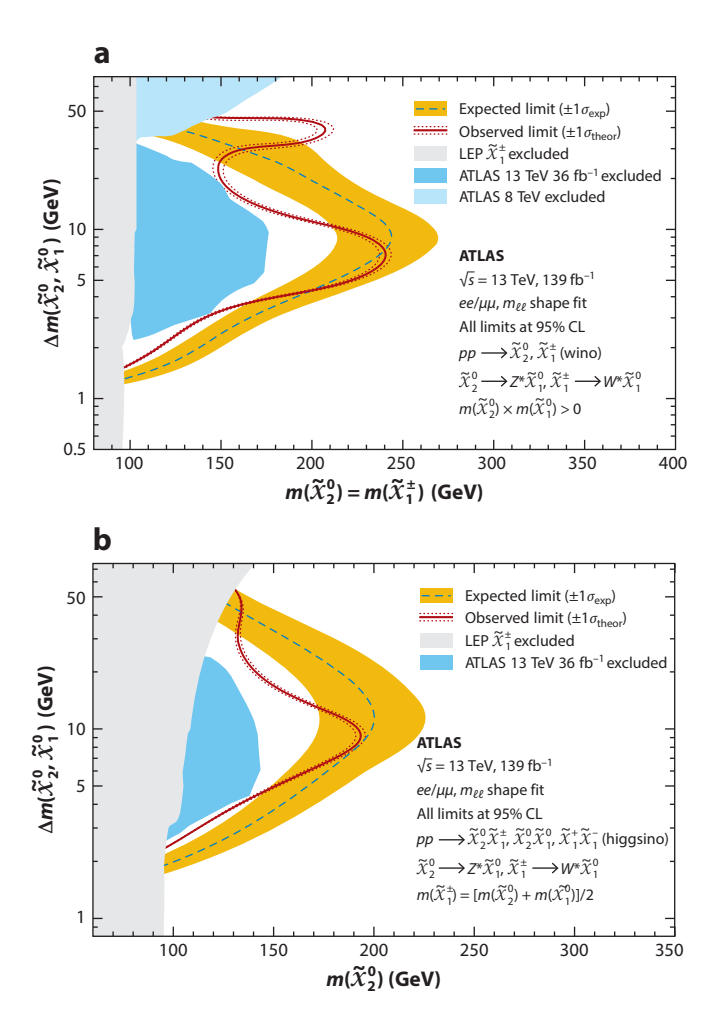


Figure 8

Expected 95% CL exclusion sensitivity with $\pm 1\sigma_{\rm exp}$ from experimental systematic uncertainties and statistical uncertainties on the data yields, and observed limits with $\pm 1\sigma_{\rm theor}$ from signal cross-section uncertainties. (a) The wino-like $\tilde{\chi}_1^\pm$ and $\tilde{\chi}_2^0$ are assumed to be mass degenerate. In these models, the $m_{\ell\ell}$ shape depends on the relative sign of the $\tilde{\chi}_2^0$ and $\tilde{\chi}_1^0$ mass parameters, $m_{\tilde{\chi}_1^0} \times m_{\tilde{\chi}_2^0}$, which is assumed to be positive in this case. More details are presented in Reference 140. (b) The electroweakinos are assumed to be higgsino-like. The chargino $\tilde{\chi}_1^\pm$ mass is assumed to be halfway between the $\tilde{\chi}_2^0$ and the $\tilde{\chi}_1^0$ masses. Figure adapted from Reference 140 (CC BY 4.0).

The interpretation of the search results under the assumption of higgsino-like electroweakino production is presented in **Figure 8b**. The CMS Collaboration has documented a similar search (145) that includes an interpretation under the assumption of wino-like $\tilde{\chi}_1^{\pm}$ and $\tilde{\chi}_2^0$ [labeled soft 2ℓ (WZ) in **Figure 7b**] and within a selected region of the pMSSM (see **Figure 9a**). The latter results highlight that the LHC experiments have so far surpassed the sensitivity achieved at LEP only in a few limited regions of parameter space.

Even though the cross section for VBF production of electroweakinos is smaller than for the $q\bar{q}$ annihilation processes, the striking signature with two forward-backward jets of $p_{\rm T}\sim M_W$ enables the experiments to efficiently extract the signal from the QCD background. VBF

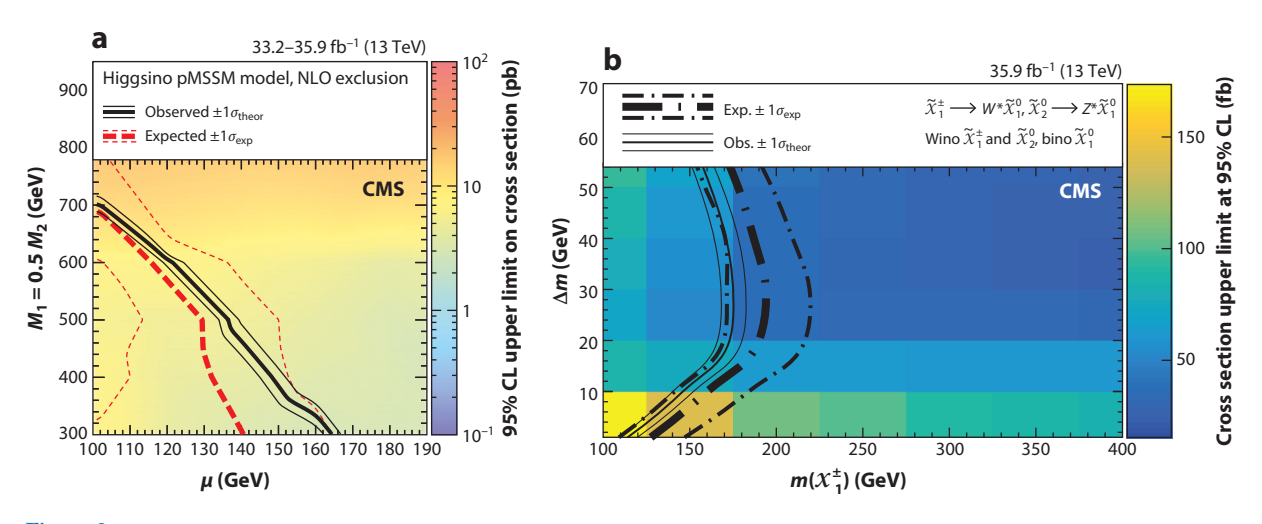
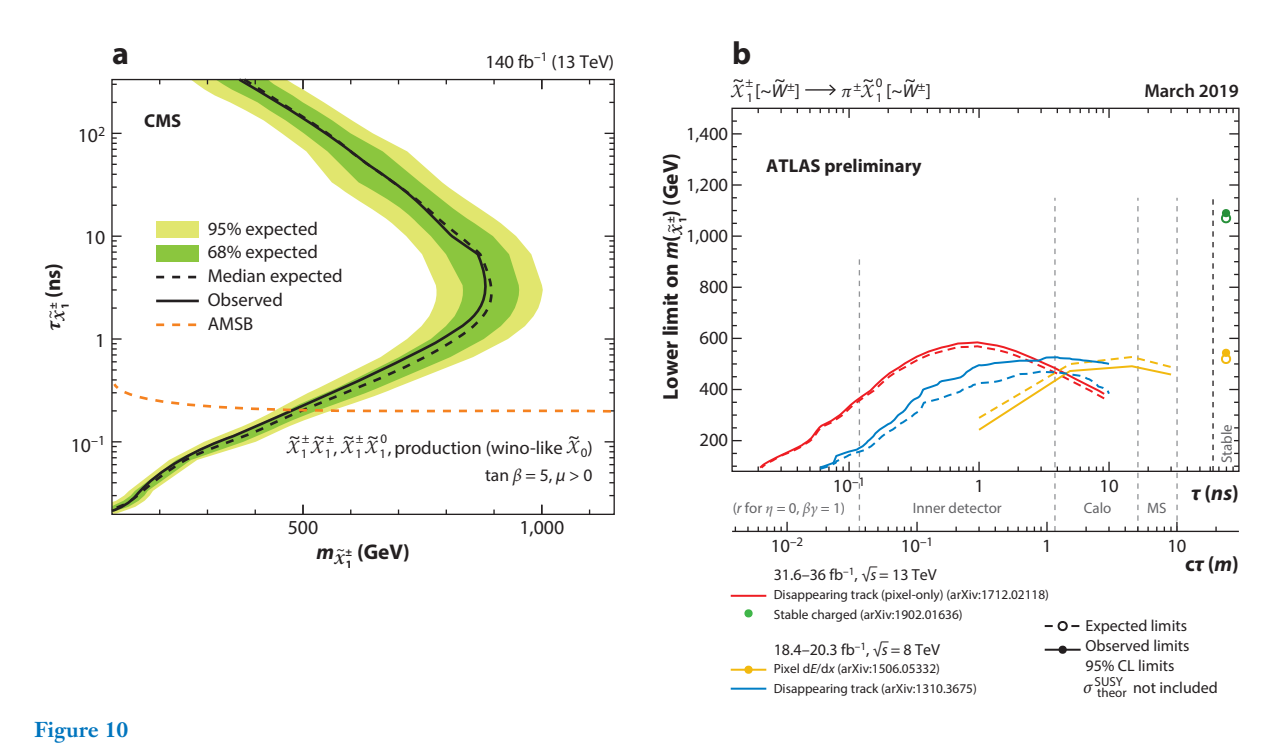


Figure 9

(a) Expected 95% CL exclusion sensitivity with $\pm 1\sigma_{\rm exp}$ from experimental systematic uncertainties and statistical uncertainties on the data yields, and observed limits with $\pm 1\sigma_{\rm theor}$ from signal cross-section uncertainties in the pMSSM described in Reference 145. (b) Expected 95% CL exclusion sensitivity with $\pm 1\sigma_{\rm exp}$ from experimental systematic uncertainties and statistical uncertainties on the data yields, and observed limits with $\pm 1\sigma_{\rm theor}$ from signal cross-section uncertainties. The colored map reports the 95% CL upper limits on the cross section. The electroweakinos are wino-like and produced via VBF. Panel a adapted from Reference 145 (CC BY 4.0). Panel b adapted from Reference 146 (CC BY 4.0).

production is usually identified by requesting two jets (j_1, j_2) with large invariant mass and large $\Delta \eta(j_1, j_2)$, reconstructed in opposite hemispheres of the detector. VBF signal events are also expected to exhibit large $p_{\rm T}^{\rm miss}$ as the $\tilde{\chi}_1^0$ from the electroweakino decays receives a boost from the two forward jets. While adopting a similar baseline event selection, the ATLAS and CMS Collaborations have developed a complementary approach to maximize the reach of their searches. In Reference 140, the ATLAS Collaboration focuses on events with two low- $p_{\rm T}$ leptons from the $\tilde{\chi}_1^{\pm} \tilde{\chi}_2^0 \to W \tilde{\chi}_1^0 Z^* \tilde{\chi}_1^0$ decays and fits the dilepton invariant mass to compute the limits in the $(\tilde{\chi}_2^0, \tilde{\chi}_1^0)$ space for both wino- and higgsino-like models. Using 139 fb⁻¹ of data, the analysis excludes wino-like and higgsino-like $\tilde{\chi}_1^{\pm}$ for masses up to ~75 GeV and ~55 GeV, respectively, depending on the $\Delta M(\tilde{\chi}_2^0, \tilde{\chi}_1^0)$ mass splitting. In Reference 146, the CMS Collaboration instead chooses events in which the electroweakinos decay either hadronically or semileptonically and probes wino-like $\tilde{\chi}_1^{\pm}$ with masses up to 112 GeV for mass splittings as small as 1 GeV (**Figure 9b**). This analysis assumes the production of $\tilde{\chi}_1^{\pm} \tilde{\chi}_2^0, \tilde{\chi}_1^{\pm} \tilde{\chi}_1^{\pm}, \tilde{\chi}_1^{\pm} \tilde{\chi}_1^{\mp}$, and $\tilde{\chi}_2^0, \tilde{\chi}_2^0$. Despite targeting a lower production cross-section process, the VBF search achieves a sensitivity comparable to that of the ISR analysis, exploring a statistically independent set of events.

4.3.4. Searches for nearly degenerate supersymmetric spectra. As introduced in Sections 2.2 and 2.3, the lifetime of electroweakinos is determined almost uniquely by the mass splitting among states. For pure higgsino states, the mass difference of 340 MeV leads to a lifetime of 0.05 ns, while the lifetime for wino states, where $\Delta M \approx 164$ MeV, is as large as 0.2 ns. In Scenarios 2 and 3, if the heavier multiplets are decoupled from the lightest one, the NLSP can become long-lived and decay into $\tilde{\chi}_1^0$ at a significant distance with respect to the production point. For lifetimes up to a few nanoseconds, the $\tilde{\chi}_1^{\pm}$ from the high-cross-section $pp \to \tilde{\chi}_1^{\pm} \tilde{\chi}_1^{\mp}$ and $pp \to \tilde{\chi}_1^{\pm} \tilde{\chi}_1^0$ processes decays in the experiments' tracker volumes as $\tilde{\chi}_1^{\pm} \to \pi^{\pm} \tilde{\chi}_1^0$, where the pion has a very low transfer momentum and cannot be reconstructed. The branching fraction is close to



(a) Expected 95% CL exclusion sensitivity (*left of the curve*) with $\pm 1\sigma_{\rm exp}$ from experimental systematic uncertainties and statistical uncertainties on the data yields, and observed limits (147). AMSB data from Reference 50. (b) Constraints on the $\tilde{\chi}_1^{\pm}$ mass–lifetime plane for an AMSB model. In this model, the wino-like chargino is pair produced and decays as $\tilde{\chi}_1^{\pm} \to \pi \tilde{\chi}_1^0$ into a wino-like $\tilde{\chi}_1^0$. It is important to note that the analyses have sensitivity at lifetimes other than those shown, but only the limits at tested lifetimes are shown. Panel *a* adapted from Reference 147 (CC BY 4.0). Panel *b* adapted from https://atlas.web.cern.ch/Atlas/GROUPS/PHYSICS/PUBNOTES/ATL-PHYS-PUB-2020-013/ (CC BY 4.0).

100%. This decay therefore leads to a peculiar signature of a track with hits only in the innermost layers and no hits in the portions of the tracker at larger radii (i.e., the disappearing track). In a recent analysis (147), the CMS Collaboration selects events that contain a disappearing track along with an ISR jet, boosting the sparticle system and producing significant $p_{\rm T}^{\rm miss}$. The disappearing track candidate is required to be compatible with the collision vertex and to have no missing inner and middle hits (147) to reduce the otherwise dominant background from spurious tracks due to pattern recognition errors. The background from leptons originating in W and Z decays is suppressed by ensuring that the candidate track is spatially separated from reconstructed leptons. The results of this search, presented in **Figure 10a**, indicate that pure winos with lifetimes of 3 and 0.2 ns are excluded up to masses of 884 and 474 GeV, respectively. The disappearing track search is also sensitive to the production of higgsinos via $pp \to \tilde{\chi}_1^{\pm} \tilde{\chi}_1^{\mp}$ and $pp \to \tilde{\chi}_1^{\pm} \tilde{\chi}_2^{0}$. In this case, the branching ratio of the $\tilde{\chi}_1^{\pm}$ is modified because of the presence of the almost-mass-degenerate $\tilde{\chi}_2^{0}$ as $\mathrm{BF}(\tilde{\chi}_1^{\pm} \to \pi \tilde{\chi}_1^{0}) = 95.5\%$, $\mathrm{BF}(\tilde{\chi}_1^{\pm} \to e\nu_e \tilde{\chi}_2^{0} \tilde{\chi}_1^{0}) = 3\%$, and $\mathrm{BF}(\tilde{\chi}_1^{\pm} \to \mu\nu_e \tilde{\chi}_2^{0} \tilde{\chi}_1^{0}) = 1.5\%$. Under these assumptions, the analysis probes $\tilde{\chi}_1^{\pm}$ masses as high as 750 and 175 GeV for lifetimes of 3 and 0.05 ns, respectively.

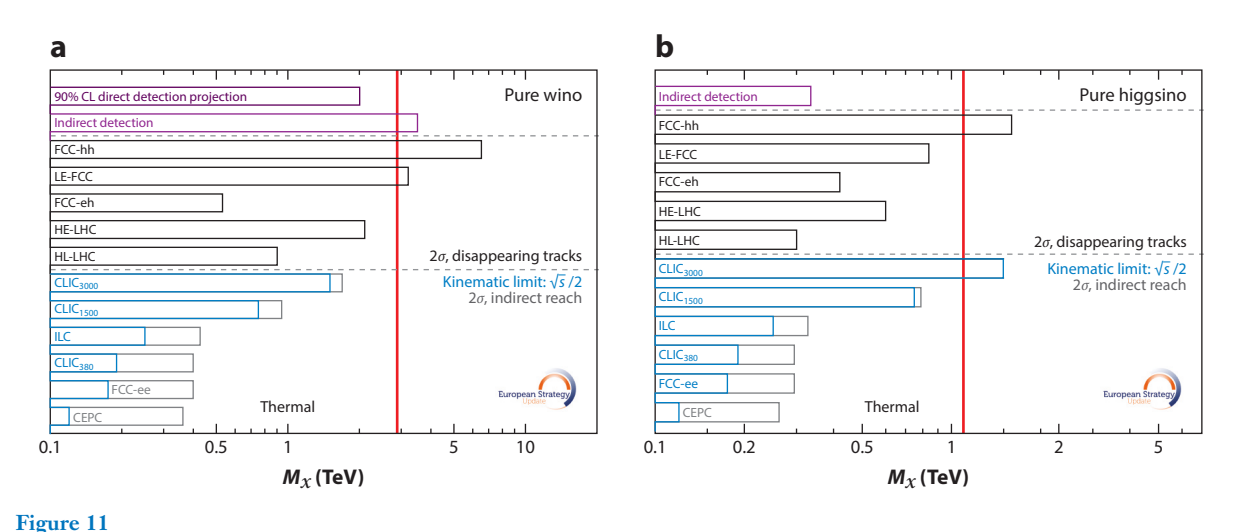
If the electroweakino is stable on the scale of the detector, the sensitivity of the disappearing track searches deteriorates since the $\tilde{\chi}_1^{\pm}$ traverses the entire tracker, leaving hits on all layers: Experimental techniques designed to detect massive charged particles moving at a speed significantly lower than the speed of light are adopted. In Reference 148, the ATLAS Collaboration exploits

the ionization energy loss and time of flight of the candidate particle (identified as a high-quality track) to determine the particle's mass, which is then used as the main observable to discriminate the signal from the background. The analysis is carried out in events with an ISR jet and significant $p_{\rm T}^{\rm miss}$. Sensitivity to stable winos with masses below 1,090 GeV is achieved, as shown in **Figure 10b**. Results from a previous ATLAS search (149), carried out in 8-TeV data, indicate that analyses based on ionization energy losses offer sensitivity to metastable winos as well (**Figure 10b**).

4.4. Expected Sensitivity at Future Colliders

A significant body of work has been produced in preparation for the European Particle Physics Strategy Update (2018–2020). Below, we summarize the most salient results; for more details, we invite readers to consult Reference 89 and the references therein.

Electron–positron linear colliders typically offer sensitivity to electroweakinos as heavy as $\sqrt{s}/2$, where s is the accelerator center-of-mass energy. For proton–proton colliders, the sensitivity is determined as a projection of results from searches carried out using LHC data as well as from dedicated analyses that use either a parameterization of the detector performance tuned to full simulation or Delphes, a fast multipurpose detector response simulation (150). It is likely that further optimization of these searches may improve the sensitivity demonstrated so far. As of the time of writing, the FCC-hh is expected to exclude wino-like $\tilde{\chi}_1^+$ and $\tilde{\chi}_2^0$ as heavy as 3.3 TeV in noncompressed scenarios with massless $\tilde{\chi}_1^0$. The HL-LHC and HE-LHC yield sensitivity to heavy electroweakinos with masses of 1 and 2 TeV, respectively. The sensitivity at the HE-LHC is comparable to that of the FCC-hh if the $\tilde{\chi}_1^+, \tilde{\chi}_2^0$ masses are smaller than 2 TeV and the $\tilde{\chi}_1^0$ mass is close to 1 TeV. For higgsino-like electroweakinos, the HL-LHC will probe the parameter space with electroweakinos lighter than 350 GeV and mass splittings larger than a few GeV. The reach of the HE-LHC is 60% higher. The FCC-hh can yield sensitivity to higgsino-like electroweakinos as heavy as 1.3 TeV for mass splittings of 20 TeV. Figure 11 provides an overview of the reach of future colliders for pure wino (Figure 11a) and pure higgsino (Figure 11b) states. The HL-LHC



Summary of the 2σ sensitivity reach to pure winos (a) and pure higgsinos (b) at future colliders. The vertical red line in each panel indicates the mass corresponding to the dark matter thermal relic. Figure adapted from Reference 89 (CC BY 4.0).

and HE-LHC can cover the parameter space characterized by pure winos as heavy as 1 and 2 TeV, respectively, while the FCC-hh extends the sensitivity above 6 TeV and thus uniquely tests the hypothesis of thermal DM. For higgsinos, mass hypotheses up to 300 and 500 GeV are tested at the HL-LHC and HE-LHC, respectively, and mass hypotheses up to approximately 1.5 TeV are tested at the FCC-hh. In the case of higgsinos, both the FCC-hh and CLIC₃₀₀₀ yield sensitivity to a large part of the parameter space in the WIMP thermal relic model.

5. SUMMARY AND FUTURE PROSPECTS

Weak-scale SUSY is one of the top contenders for BSM physics. In this review, we have considered a general theoretical framework for fermionic color-singlet states—including a singlet, a doublet, and a triplet under the SM SU(2)_L gauge symmetry, corresponding to the bino, higgsino, and wino in SUSY theories—generically dubbed electroweakinos for their mass eigenstates.

Assuming R parity conservation, no new sources of CP violation, and decoupling of the SUSY scalar and color states, the electroweakino sector is simply specified by the three mass parameters M_1 , M_2 , and μ plus $\tan \beta$. Those parameters govern the phenomenology and the observable signatures: The lighter parameter determines the LSP mass, the heavier one tends to decouple, and those with a similar value will lead to substantial state mixing. R parity conservation leads to the stability of the LSP state that can be a natural cold DM candidate.

The ATLAS and CMS experiments have pushed the boundaries of knowledge for electroweakino searches thanks to the outstanding performance of the LHC and the experiments themselves. Breakthrough analytical techniques have made it possible to achieve great sensitivity:

- Under the assumption of noncompressed scenarios, wino-like electroweakinos decaying into higgsino- or bino-like LSPs are excluded at the 95% CL for masses of 600 to 700 GeV if the $\tilde{\chi}_1^0$ is massless.
- The sensitivity to both wino- and higgsino-like $\tilde{\chi}_1^{\pm}$ and $\tilde{\chi}_2^0$ in compressed scenarios is challenged by the complexity of reconstructing low- p_T objects and reaches a few hundred GeV for ΔM between 10 and 50 GeV, but quickly drops for mass splittings between a few GeV and a few hundred MeV.
- Scenarios with pure higgsino and pure wino electroweakinos, characterized by ΔM on the order of hundreds of MeV, are probed up to a scale of 700 to 800 GeV for lifetimes of a few nanoseconds.
- The reach for stable sparticles is on the order of 1 TeV.
- Models predicting metastable electroweakinos with lifetimes between a few nanoseconds and hundreds of nanoseconds, as well as those leading to short-lived sparticles, have not been fully explored yet.

Looking forward, innovative ideas and experimental strategies are being devised by both the ATLAS and CMS Collaborations to extend the reach to challenging regions of parameter space—for instance, by searching for long-lived sparticles as well as for promptly decaying electroweakinos with ΔM in the mass range of a few GeV to a few hundred MeV. Furthermore, the fast development of boosted boson identification (W, Z, H) is enabling the search for heavier electroweakinos in noncompressed spectra.

It is worth noting that the quoted limits are set at the 95% CL and are valid in the context of simplified models, in which the electroweakinos are typically assumed to be pure states and their branching fractions in the experimental searches are set to 100%. The reinterpretation of

the search results within realistic frameworks, such as those presented in Section 2, indicates the need for further optimization of analyses to target scenarios in which electroweakinos decay in various modes. Thus, there is still ample room for discovery of electroweakinos at the LHC and HL-LHC (151–155). Furthermore, there are extensions beyond the MSSM in well-motivated theoretical frameworks, such as the singlet extension (NMSSM) (156, 157) and the inclusion of QCD axions (158, 159), that would require modification and optimization for the search strategies with additional particles.

Either the search for or the characterization of electroweakinos discovered at the LHC experiments will continue at future colliders, opening up the following possibilities:

- A future proton–proton collider at $\sqrt{s} = 100$ TeV would extend the reach well above the TeV scale, enabling probing of noncompressed spectra up to 3 TeV and the very compressed one up to 5 TeV.
- The electron–positron colliders may serve as discovery machines up to a mass as high as $\sqrt{s}/2$, a capability that is limited only by the kinematic threshold and that is essentially model independent. Such colliders especially complement the hadron machines in parameter space with compressed SUSY spectra, where the signal observation would be challenging at hadron colliders.

The direct detections of WIMP DM in underground experiments have achieved very impressive sensitivity, reaching SI cross sections of 10^{-46} cm² for the favorable mass region $m_{\tilde{\chi}_1^0} \sim 10$ GeV. At lower masses, the sensitivity drops because of the lack of detectable recoil energy, while the collider searches for electroweakinos nicely complement these searches because of the larger missing kinetic energy for a lighter missing particle. The direct detection sensitivity also drops for a TeV-mass DM because of the lower signal rate, while once again the heavy DM searches at future colliders will be further improved because of the accessible phase space at higher energies. Ideally, the two complementary searches should observe consistent signals to confirm the discovery of a WIMP DM particle.

The search for electroweakinos presented in this review provides a well-defined experimental target within a general and well-motivated theoretical framework; thus, it holds great promise for future discoveries.

DISCLOSURE STATEMENT

The authors are not aware of any affiliations, memberships, funding, or financial holdings that might be perceived as affecting the objectivity of this review.

ACKNOWLEDGMENTS

We would like to thank Tathagata Ghosh, Zhen Liu, Xerxes Tata, and Lian-Tao Wang for comments on the manuscript. T.H. was supported in part by the US Department of Energy under grant DE-FG02-95ER40896 and in part by the PITT PACC. X.W. was supported by the National Science Foundation (NSF) under grant PHY-1915147. We would also like to thank the Aspen Center for Physics, where part of the work was completed, for hospitality. The Aspen Center for Physics is supported by the NSF under grant PHYS-1066293. We thank the ATLAS and CMS Collaborations for their contributions to the search for SUSY at the LHC. This manuscript has been authored by Fermi Research Alliance, LLC, under contract DE-AC02-07CH11359 with the US Department of Energy, Office of Science, Office of High Energy Physics.

LITERATURE CITED

- 1. Aad G, et al. *Phys. Lett. B* 716:1 (2012)
- 2. Chatrchyan S, et al. Phys. Lett. B 716:30 (2012)
- 3. Weinberg S. Phys. Rev. D 13:974 (1976). Addendum. Phys. Rev. D 19:1277 (1979)
- 4. Gildener E. Phys. Rev. D 14:1667 (1976)
- 5. Susskind L. Phys. Rev. D 20:2619 (1979)
- 6. 't Hooft G, et al. NATO Sci. Ser. B 59:1 (1980)
- 7. Ellis JR, Kelley S, Nanopoulos DV. Phys. Lett. B 260:131 (1991)
- 8. Amaldi U, de Boer W, Furstenau H. Phys. Lett. B 260:447 (1991)
- 9. Langacker P, Luo M. Phys. Rev. D 44:817 (1991)
- Giunti C, Kim CW, Lee UW. Mod. Phys. Lett. A 6:1745 (1991)
- 11. Gol'fand YA, Likhtman EP. JETP Lett. 13:323 (1971) [Pisma Zh. Eksp. Teor. Fiz. 13:452 (1971)]
- 12. Volkov DV, Akulov VP. Phys. Lett. B 46:109 (1973)
- 13. Wess J, Zumino B. Nucl. Phys. B 70:39 (1974)
- 14. Wess J, Zumino B. Nucl. Phys. B 78:1 (1974)
- 15. Ferrara S, Zumino B. Nucl. Phys. B 79:413 (1974)
- 16. Salam A, Strathdee JA. Phys. Lett. B 51:353 (1974)
- 17. Kaplan DB, Georgi H. Phys. Lett. B 136:183 (1984)
- 18. Kaplan DB, Georgi H, Dimopoulos S. Phys. Lett. B 136:187 (1984)
- 19. Georgi H, Kaplan DB. Phys. Lett. B 145:216 (1984)
- 20. Randall L, Sundrum R. Phys. Rev. Lett. 83:3370 (1999)
- 21. Randall L, Sundrum R. Phys. Rev. Lett. 83:4690 (1999)
- 22. Nilles HP. Phys. Rep. 110:1 (1984)
- 23. Haber HE, Kane GL. Phys. Rep. 117:75 (1985)
- Martin SP. arXiv:hep-ph/9709356 [hep-ph] (1997) [Martin SP. A supersymmetry primer. In Perspectives on Supersymmetry, ed. GL Kane, pp. 1–98. Singapore: World Sci. (1998)]
- Giudice GF. Naturally speaking: the naturalness criterion and physics at the LHC. In Perspectives on LHC Physics, ed. G Kane, pp. 155–78. Singapore: World Sci. (2008)
- 26. Feng JL. Annu. Rev. Nucl. Part. Sci. 63:351 (2013)
- 27. Jungman G, Kamionkowski M, Griest K. Phys. Rep. 267:195 (1996)
- ATLAS Collab. ATLAS experiment—public results: supersymmetry searches. Public data, ATLAS Collab., CERN, Geneva. https://twiki.cern.ch/twiki/bin/view/AtlasPublic/SupersymmetryPublicResults (2020)
- CMS Collab. CMS supersymmetry physics results. Public data, CMS Collab., CERN, Geneva. https://twiki.cern.ch/twiki/bin/view/CMSPublic/PhysicsResultsSUS (2020)
- 30. Sirunyan AM, et al. 7. High Energy Phys. 1910:244 (2019)
- 31. ATLAS Collab. Search for squarks and gluinos in final states with jets and missing transverse momentum using 139 fb⁻¹ of√s = 13 TeV pp collision data with the ATLAS detector. Tech. Rep. ATLAS-CONF-2019-040, CERN, Geneva (2019)
- 32. Feng JL, Matchev KT, Moroi T. Phys. Rev. D 61:075005 (2000)
- 33. Hall LJ, Pinner D, Ruderman JT. 7. High Energy Phys. 1204:131 (2012)
- 34. Baer H, et al. Phys. Rev. Lett. 109:161802 (2012)
- 35. Baer H, et al. arXiv:2002.03013 [hep-ph] (2020)
- 36. Baer H, Chen C, Paige F, Tata X. Phys. Rev. D 50:4508 (1994)
- 37. Athron P, et al. Eur. Phys. 7. C 79:395 (2019)
- 38. Arkani-Hamed N, Delgado A, Giudice GF. Nucl. Phys. B 741:108 (2006)
- 39. Giudice GF, Han T, Wang K, Wang LT. Phys. Rev. D 81:115011 (2010)
- 40. Chamseddine AH, Arnowitt RL, Nath P. Phys. Rev. Lett. 49:970 (1982)
- 41. Barbieri R, Ferrara S, Savoy CA. Phys. Lett. B 119:343 (1982)
- 42. Ibánez LE. Phys. Lett. B 118:73 (1982)
- 43. Hall LJ, Lykken JD, Weinberg S. *Phys. Rev. D* 27:2359 (1983)
- 44. Ohta N. Prog. Theor. Phys. 70:542 (1983)

- 45. Ellis JR, Nanopoulos DV, Tamvakis K. Phys. Lett. B 121:123 (1983)
- 46. Alvarez-Gaumé L, Polchinski J, Wise MB. Nucl. Phys. B 221:495 (1983)
- 47. Randall L, Sundrum R. Nucl. Phys. B 557:79 (1999)
- 48. Giudice GF, Luty MA, Murayama H, Rattazzi R. 7. High Energy Phys. 9812:027 (1998)
- 49. Gherghetta T, Giudice GF, Wells JD. Nucl. Phys. B 559:27 (1999)
- 50. Ibe M, Matsumoto S, Sato R. Phys. Lett. B 721:252 (2013)
- 51. Fukuda H, Nagata N, Otono H, Shirai S. Phys. Lett. B 781:306 (2018)
- 52. Chung DJH, et al. Phys. Rep. 407:1 (2005)
- 53. Dine M, Fischler W. Phys. Lett. B 110:227 (1982)
- 54. Nappi CR, Ovrut BA. Phys. Lett. B 113:175 (1982)
- 55. Alvarez-Gaumé L, Claudson M, Wise MB. Nucl. Phys. B 207:96 (1982)
- 56. Dine M, Nelson AE. Phys. Rev. D 48:1277 (1993)
- 57. Dine M, Nelson AE, Shirman Y. Phys. Rev. D 51:1362 (1995)
- 58. Dine M, Nelson AE, Nir Y, Shirman Y. Phys. Rev. D 53:2658 (1996)
- 59. Giudice GF, Rattazzi R. Phys. Rep. 322:419 (1999)
- 60. Arbey A, et al. Phys. Lett. B 708:162 (2012)
- 61. Ajaib MA, Gogoladze I, Nasir F, Shafi Q. Phys. Lett. B 713:462 (2012)
- 62. Kang Z, et al. Phys. Rev. D 86:095020 (2012)
- 63. Craig N, Knapen S, Shih D, Zhao Y. J. High Energy Phys. 1303:154 (2013)
- 64. Albaid A, Babu KS. Phys. Rev. D 88:055007 (2013)
- 65. Cohen T, Lisanti M, Pierce A, Slatyer TR. J. Cosmol. Astropart. Phys. 1310:061 (2013)
- 66. Alwall J, Schuster P, Toro N. Phys. Rev. D 79:075020 (2009)
- 67. Alves D. J. Phys. G 39:105005 (2012)
- 68. Berger CF, Gainer JS, Hewett JL, Rizzo TG. J. High Energy Phys. 0902:023 (2009)
- 69. Lee BW, Weinberg S. Phys. Rev. Lett. 39:165 (1977)
- 70. Goldberg H. Phys. Rev. Lett. 50:1419 (1983). Erratum. Phys. Rev. Lett. 103:099905 (2009)
- 71. Steigman G, Dasgupta B, Beacom JF. Phys. Rev. D 86:023506 (2012)
- 72. Bramante J, et al. *Phys. Rev. D* 93:063525 (2016)
- 73. Griest K, Seckel D. Phys. Rev. D 43:3191 (1991)
- 74. Mizuta S, Yamaguchi M. Phys. Lett. B 298:120 (1993)
- 75. Edsjo J, Gondolo P. Phys. Rev. D 56:1879 (1997)
- 76. Baer H, Balazs C, Belyaev A. 7. High Energy Phys. 0203:042 (2002)
- 77. Boehm C, Djouadi A, Drees M. Phys. Rev. D 62:035012 (2000)
- 78. Ellis JR, Olive KA, Santoso Y. Astropart. Phys. 18:395 (2003)
- 79. Arnowitt RL, Dutta B, Santoso Y. Nucl. Phys. B 606:59 (2001)
- 80. Ellis JR, Falk T, Olive KA. Phys. Lett. B 444:367 (1998)
- Ellis JR, Falk T, Olive KA, Srednicki M. Astropart. Phys. 13:181 (2000). Erratum. Astropart. Phys. 15:413 (2001)
- 82. Gómez ME, Lazarides G, Pallis C. Phys. Rev. D 61:123512 (2000)
- 83. Nihei T, Roszkowski L, Ruiz de Austri R. J. High Energy Phys. 07:024 (2002)
- 84. Baer H, et al. 7. High Energy Phys. 0512:011 (2005)
- 85. Berlin A, Gori S, Lin T, Wang LT. Phys. Rev. D 92:015005 (2015)
- 86. Freese K, López A, Shah NR, Shakya B. J. High Energy Phys. 1604:59 (2016)
- 87. Gilmore RC. Phys. Rev. D 76:043520 (2007)
- 88. Kar A, Mitra S, Mukhopadhyaya B, Choudhury TR. Phys. Rev. D 99:021302 (2019)
- 89. Ellis RK, et al. (Eur. Strateg. Part. Phys. Prep. Group) arXiv:1910.11775 [hep-ex] (2019)
- Cushman P, et al. Snowmass CF1 summary: WIMP dark matter direct detection. Presented at 2013 Community Summer Study on the Future of U.S. Particle Physics: Snowmass on the Mississippi (CSS2013), Minneapolis, MN, July 29–Aug. 6 (2013)
- 91. Hisano J, Ishiwata K, Nagata N. J. High Energy Phys. 1506:97 (2015)
- 92. Chen Q, Hill RJ. Phys. Lett. B 804:135364 (2020)
- 93. Cheung C, Hall LJ, Pinner D, Ruderman JT. J. High Energy Phys. 1305:100 (2013)

- 94. Han T, Kling F, Su S, Wu Y. 7. High Energy Phys. 1702:57 (2017)
- 95. Huang P, Wagner CEM. Phys. Rev. D 90:015018 (2014)
- 96. Baum S, Carena M, Shah NR, Wagner CEM. J. High Energy Phys. 1804:69 (2018)
- 97. Han T, Liu H, Mukhopadhyay S, Wang X. 7. High Energy Phys. 1903:80 (2019)
- 98. Choi SY, et al. Eur. Phys. 7. C 7:123 (1999)
- Choi SY, Kalinowski J, Moortgat-Pick GA, Zerwas PM. Eur. Phys. J. C 22:563 (2001). Addendum. Eur. Phys. J. C 23:769 (2002)
- 100. Aarons G, et al. arXiv:0709.1893 [hep-ph] (2007)
- 101. Arbey A, et al. Eur. Phys. J. C 75:371 (2015)
- 102. Carena M, Wagner CEM. Phys. Lett. B 195:599 (1987)
- 103. Chen CH, Drees M, Gunion JF. Phys. Rev. Lett. 76:2002 (1996)
- 104. Hensel C. Search for nearly mass degenerate charginos and neutralinos in e⁺e⁻ collisions. PhD Diss., Hamburg Univ., Hamburg, Ger. (2002)
- 105. Berggren M, et al. Eur. Phys. 7. C 73:2660 (2013)
- 106. Birkedal A, Matchev K, Perelstein M. Phys. Rev. D 70:077701 (2004)
- 107. Dreiner H, et al. Phys. Rev. D 87:075015 (2013)
- 108. Lebrun P, et al. arXiv:1209.2543 [physics.ins-det] (2012)
- 109. Tanabashi M, et al. Phys. Rev. D 98:030001 (2018)
- 110. Dreiner HK, et al. Eur. Phys. 7. C 62:547 (2009)
- 111. de Filippis N, et al. (LEP2 SUSY Work. Group) Combined LEP chargino results, up to 208 GeV: ALEPH, DELPHI, L3, OPAL experiments. Rep. LEPSUSYWG/02-04.1, CERN, Geneva. http://lepsusy.web.cern.ch/lepsusy/www/inoslowdmsummer02/charginolowdm_pub.html (2002)
- 112. Han T, Padhi S, Su S. Phys. Rev. D 88:115010 (2013)
- 113. Lee BW, Quigg C, Thacker HB. Phys. Rev. D 16:1519 (1977)
- 114. Chanowitz MS, Gaillard MK. Nucl. Phys. B 261:379 (1985)
- 115. Bagger J, Schmidt C. Phys. Rev. D 41:264 (1990)
- 116. He HJ, Kuang YP, Li X. Phys. Rev. Lett. 69:2619 (1992)
- 117. Gori S, Liu Z, Shakya B. 7. High Energy Phys. 1904:49 (2019)
- 118. Datta A, Konar P, Mukhopadhyaya B. Phys. Rev. D 65:055008 (2002)
- 119. Datta A, Konar P, Mukhopadhyaya B. Phys. Rev. Lett. 88:181802 (2002)
- 120. Cho GC, et al. Phys. Rev. D 73:054002 (2006)
- 121. Dutta B, et al. Phys. Rev. D 87:035029 (2013)
- 122. Cotta RC, Hewett JL, Le MP, Rizzo TG. Phys. Rev. D 88:116009 (2013)
- 123. Delannoy AG, et al. Phys. Rev. Lett. 111:061801 (2013)
- 124. Cowan G, Cranmer K, Gross E, Vitells O. Eur. Phys. 7. C 73:2501 (2013)
- 125. Junk T. Nucl. Instr. Meth. A 434:435 (1999)
- 126. Read AL. J. Phys. G 28:2693 (2002)
- Cowan G, Cranmer K, Gross E, Vitells O. Eur. Phys. J. C 71:1554 (2011). Erratum. Eur. Phys. J. C 73:2501 (2013)
- 128. Aad G, et al. (ATLAS Collab.) arXiv:1909.09226 [hep-ex] (2019)
- 129. Aaboud M, et al. Phys. Rev. D 100:012006 (2019)
- 130. Sirunyan AM, et al. 7. High Energy Phys. 1711:29 (2017)
- Sirunyan AM, et al. J. High Energy Phys. 1911:109 (2019)
- 132. Sirunyan AM, et al. *7. High Energy Phys.* 1803:76 (2018)
- 133. Barr A, Lester C, Stephens P. J. Phys. G 29:2343 (2003)
- 134. Aaboud M, et al. Phys. Rev. D 98:092012 (2018)
- 135. Aad G, et al. (ATLAS Collab.) Eur. Phys. 7. C 80:123 (2020)
- ATLAS Collab. Object-based missing transverse momentum significance in the ATLAS detector. ATLAS Note ATLAS-CONF-2018-038, CERN, Geneva. https://cds.cern.ch/record/2630948 (2018)
- 137. Sirunyan AM, et al. J. High Energy Phys. 1803:166 (2018)
- 138. Sirunyan AM, et al. 7. High Energy Phys. 1803:160 (2018)
- 139. Aaboud M, et al. Eur. Phys. 7. C 78:995 (2018)

- 140. Aad G, et al. (ATLAS Collab.) Phys. Rev. D 101:052005 (2020)
- 141. Han Z, Kribs GD, Martin A, Menon A. Phys. Rev. D 89:075007 (2014)
- 142. Baer H, Mustafayev A, Tata X. Phys. Rev. D 90:115007 (2014)
- 143. Barr A, Scoville J. J. High Energy Phys. 1504:147 (2015)
- 144. Jackson P, Rogan C. Phys. Rev. D 96:112007 (2017)
- 145. Sirunyan AM, et al. Phys. Lett. B 782:440 (2018)
- 146. Sirunyan AM, et al. J. High Energy Phys. 1908:150 (2019)
- 147. Sirunyan AM, et al. (CMS Collab.) Phys. Lett. B 806:135502 (2020)
- 148. Aaboud M, et al. Phys. Rev. D 99:092007 (2019)
- 149. Aad G, et al. Eur. Phys. J. C 75:407 (2015)
- 150. de Favereau J, et al. J. High Energy Phys. 1402:57 (2014)
- 151. Aad G, et al. Phys. Rev. D 93:052002 (2016)
- 152. Aad G, et al. J. High Energy Phys. 1510:54 (2015)
- 153. Aad G, et al. Eur. Phys. J. C 75:510 (2015). Erratum. Eur. Phys. J. C 76:153 (2016)
- 154. Aad G, et al. J. High Energy Phys. 1510:134 (2015)
- 155. Khachatryan V, et al. J. High Energy Phys. 1610:129 (2016)
- 156. Ellis JR, et al. Phys. Rev. D 39:844 (1989)
- 157. Drees M. Int. J. Mod. Phys. A 4:3635 (1989)
- 158. Kim JE, Nilles HP. Phys. Lett. B 138:150 (1984)
- 159. Baer H, Choi KY, Kim JE, Roszkowski L. Phys. Rep. 555:1 (2015)



Annual Review of Nuclear and Particle Science

Volume 70, 2020

Contents

"Why Do We Do Physics? Because Physics Is Fun!" *James D. Bjorken
Covariant Density Functional Theory in Nuclear Physics and Astrophysics Junjie Yang and J. Piekarewicz
Parton Distributions in Nucleons and Nuclei *Jacob J. Ethier and Emanuele R. Nocera**
The Shortage of Technetium-99m and Possible Solutions Thomas J. Ruth
The Dynamics of Binary Neutron Star Mergers and GW170817 David Radice, Sebastiano Bernuzzi, and Albino Perego
Theoretical Prediction of Presupernova Neutrinos and Their Detection C. Kato, K. Ishidoshiro, and T. Yoshida
Nuclear Reactions in Astrophysics: A Review of Useful Probes for Extracting Reaction Rates F.M. Nunes, G. Potel, T. Poxon-Pearson, and J.A. Cizewski
Tracking Triggers for the HL-LHC Anders Ryd and Louise Skinnari
Extended Scalar Sectors **Jan Steggemann** 197
What Is the Top Quark Mass? André H. Hoang
The Nuclear Legacy Today of Fukushima <i>Kai Vetter</i>
Chiral Magnetic Effects in Nuclear Collisions Wei Li and Gang Wang
Photonuclear and Two-Photon Interactions at High-Energy Nuclear Colliders
Spencer R. Klein and Peter Steinberg 323

Primordial Black Holes as Dark Matter: Recent Developments *Bernard Carr and Florian Kühnel	355
Polarization and Vorticity in the Quark–Gluon Plasma Francesco Becattini and Michael A. Lisa	395
The Search for Electroweakinos Anadi Canepa, Tao Han, and Xing Wang	425
The Fermi–LAT Galactic Center Excess: Evidence of Annihilating Dark Matter?	
Simona Murgia	455

Errata

An online log of corrections to *Annual Review of Nuclear and Particle Science* articles may be found at http://www.annualreviews.org/errata/nucl